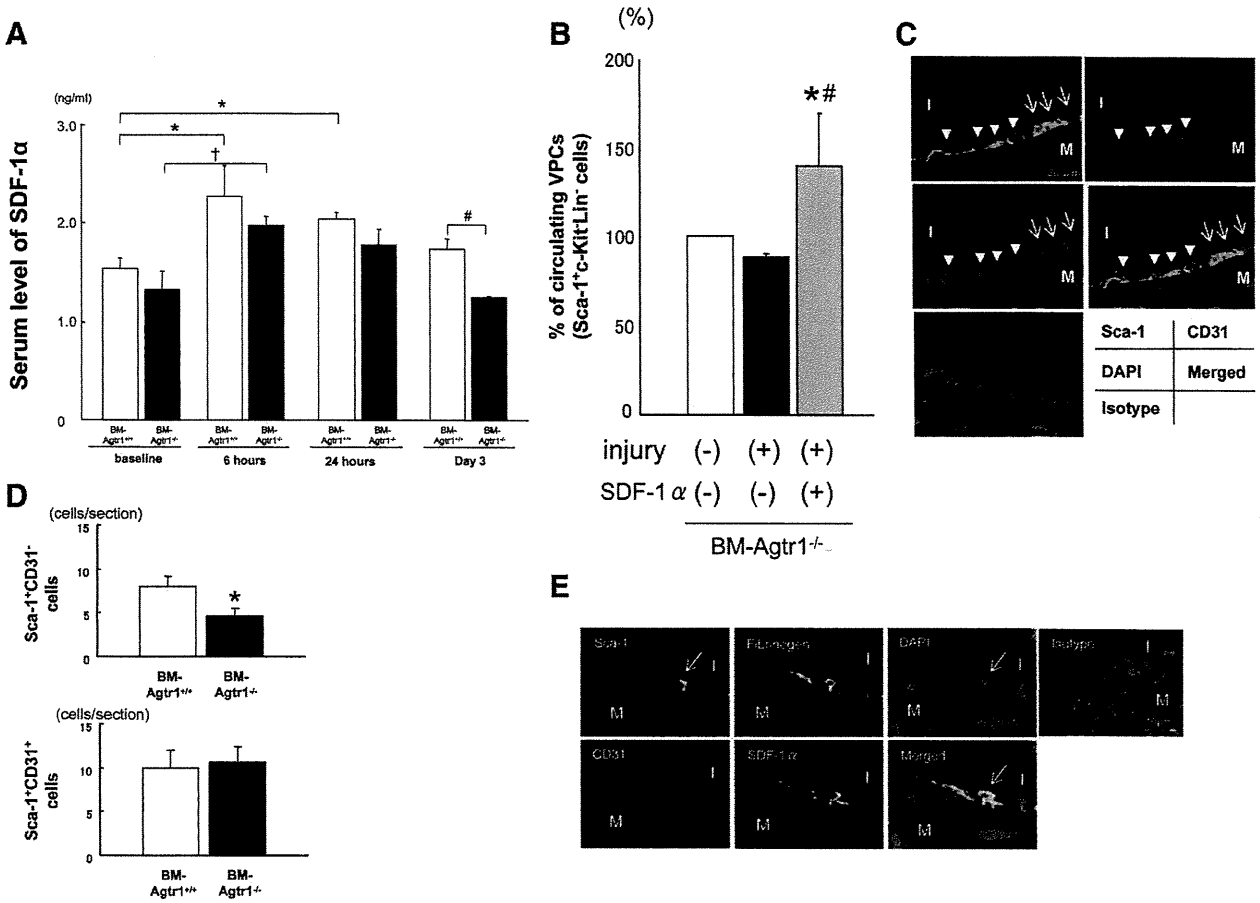

Figure 4. Decrease in the serum level of SDF-1α accompanied by the decreased number of Sca-1$^+$CD31$^-$ cells incorporated into neointima on ablation of marrow AT_1. A, The serum SDF-1α level was markedly increased after injury with a peak of 6 hours in both groups. In the BM-Agtr1$^{-/-}$ mice, the serum SDF-1α level rapidly declined and normalized at 3 days after injury, which was significantly lower than that in BM-Agtr1$^{+/+}$ mice. Values are the mean±SE for at least 4 mice in each group. *P<0.01 vs BM-Agtr1$^{+/+}$ mice before injury. †P<0.01 vs BM-Agtr1$^{-/-}$ mice before injury, #P<0.05 vs BM-Agtr1$^{+/+}$ mice 3 days after injury. B, BM-Agtr1$^{-/-}$ mice were injected with SDF-1α (10 μg i.p.) 1 day after injury. Flow cytometry of c-Kit and Sca-1 expression in lineage-negative populations was performed on day 3 after injury. The bar graphs represent the mean±SE relative to BM-Agtr1$^{-/-}$ before injury set at 100%. At least 5 mice were tested in each group. *P<0.05 vs BM-Agtr1$^{-/-}$ mice before injury. #P<0.05 vs BM-Agtr1$^{-/-}$ mice after injury. C, Immunofluorescence image showing Sca-1 (green), CD31 (red), and DAPI (blue) 7 days after injury. Arrows indicate Sca-1$^+$CD31$^-$ cells, and arrowheads indicate Sca-1$^+$CD31$^+$. D, Quantitative analysis showed that the number of Sca-1$^+$CD31$^-$ cells was significantly reduced in BM-Agtr1$^{-/-}$ mice, whereas no difference was observed in Sca-1$^+$CD31$^+$ cells between the 2 groups. Values are the mean±SE for at least 4 mice in each group. *P<0.05 vs BM-Agtr1$^{+/+}$ mice. I indicates intima; M, media. E, Immunofluorescence image showing VPC (arrow) which was colocalized with fibrinogen-positive staining (cyan blue), that reflects the fibrinogen trapped by aggregated platelets, and SDF-1α (yellow).

BM-Agtr1$^{-/-}$ mice declined more rapidly and normalized 24 hours after injury and thereafter further decreased. SDF-1α–positive staining at 3 days after injury was mostly colocalized with fibrinogen-positive staining at the inner surface of the injured artery but not the medial wall (Figure 3D). These findings suggest that a main source of serum SDF-1α after injury was medial smooth muscle cells in the early phase, and that in the late phase is derived from aggregated platelets. We also examined the serum SDF-1α levels in sham operated animals 3 days after injury, and found that they were equivalent to those (baseline in Figure 4A) in unoperated animals (data not shown). These findings strongly support the notion that attenuated platelet aggregation followed by the reduced release of SDF-1α is closely involved in a rapid decline in the serum SDF-1α level, resulting in impaired mobilization of VPCs in BM-Agtr1$^{-/-}$ mice.

Impaired Mobilization of Agtr1$^{-/-}$ VPCs Is Restored by SDF-1α

We examined whether administration of SDF-1α restored the impaired mobilization of VPCs in BM-Agtr1$^{-/-}$ mice. An injection of SDF-1α into vascular-injured BM-Agtr1$^{-/-}$ mice increased the number of circulating VPCs by 44% (P<0.05), whereas vascular injury alone did not increase the number of circulating VPCs (Figure 4B). We also examined the effect of anti–SDF-1α antibody (to block CXCR4 axis) on the number of circulating VPCs. Three-day pretreatment with anti–SDF-1α antibody completely abolished the difference in the number of circulating VPCs between the 2 chimeric mice (supplemental Figure III). These findings strongly support the notion that the rapid decline in the serum SDF-1α level caused by the attenuated platelet aggregation seems to be attributable to the impaired mobilization of VPCs in BM-Agtr1$^{-/-}$ mice.

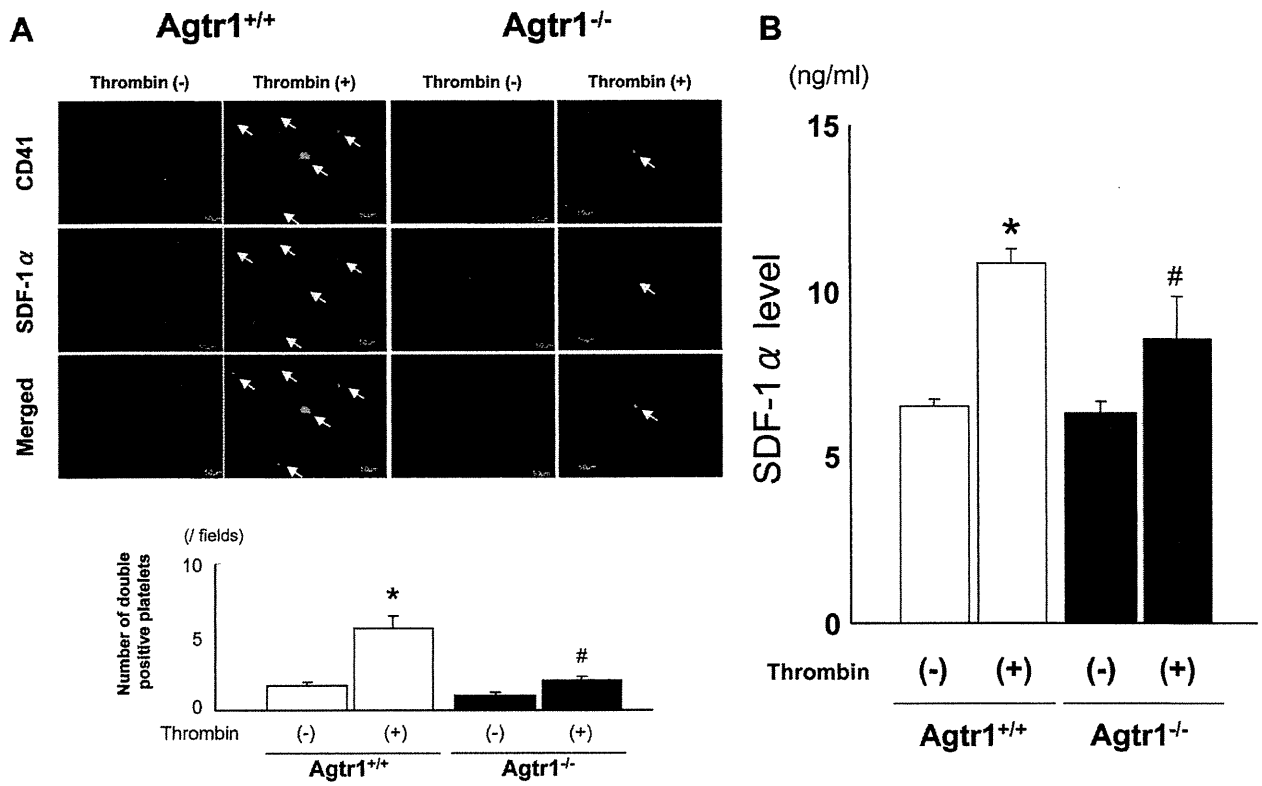

Figure 5. Attenuated platelet aggregation and thrombin-activated platelets-derived SDF-1α expression and release on ablation of marrow AT_1. A, Mice platelets were stimulated with 0.2 U/mL thrombin, fixed, and stained with FITC-labeled anti-CD41 and anti–SDF-1α. Arrows indicate $CD41^+SDF\text{-}1\alpha^+$ platelets. $CD41^+SDF\text{-}1\alpha^+$ platelets indicated by arrows were aggregated cells but not a single platelet. Quantitative analysis showed that the number of double positive platelets was significantly increased in $Agtr1^{+/+}$ platelets after stimulation with thrombin, whereas it was significantly diminished in $Agtr1^{-/-}$ platelets. *$P<0.01$ vs $Agtr1^{+/+}$ resting platelets, #$P<0.05$ vs $Agtr1^{+/+}$ activated platelets. B, Measurement of SDF-1α released from $Agtr1^{+/+}$ platelets or $Agtr1^{-/-}$ platelets after thrombin stimulation by the ELISA method. SDF-1α protein in the conditioned medium was significantly reduced in $Agtr1^{-/-}$ platelets after thrombin stimulation. Values are the mean±SE for at least 5 mice in each group. *$P<0.05$ vs $Agtr1^{+/+}$ resting platelets. #$P<0.05$ vs $Agtr1^{+/+}$ activated platelets.

BM-AT_1 Deficiency Attenuates the Homing of VPCs

To examine the homing of VPCs, the vascular localization of VPCs was evaluated at day 7 after injury. As shown in Figure 4C and 4E, vascular $Sca\text{-}1^+CD31^-$ cells (arrows), corresponding to VPCs,[8] were colocalized with aggregated platelets which express SDF-1α. The number of VPCs, was markedly reduced by 42% in BM-$Agtr1^{-/-}$ mice compared with BM-$Agtr1^{+/+}$ mice ($P<0.05$) (Figure 4D). In contrast, the number of $Sca\text{-}1^+CD31^+$ cells, corresponding to EPCs,[7] did not differ between the 2 groups, suggesting that BM-AT_1 deficiency attenuates the homing of BM-derived progenitor cells concomitant with the impaired mobilization of VPCs.

Platelet AT_1 Receptor Deficiency Inhibits Platelet Aggregation

Thrombin-stimulated $Agtr1^{+/+}$ platelets showed an apparent increase in fibrinogen binding in a dose-dependent manner, whereas fibrinogen binding in $Agtr1^{-/-}$ platelets was significantly reduced (45% at 0.1 IU/mL, $P<0.05$; supplemental Figure IVA and IVB), which was consistent with the previous data showing that ARB treatment significantly reduced platelet aggregation.[16] Platelets produce reactive oxidative species (ROS) via NAD(P)H oxidase activation, and their function is tightly regulated by the redox state.[17] We examined whether production of ROS is actually reduced in $Agtr1^{-/-}$ platelets. Intracellular ROS production, which was detected by flow cytometric analysis with H_2DCF-DA, showed a significant decrease in $Agtr1^{-/-}$ platelets by 37% ($P<0.01$) compared with $Agtr1^{+/+}$ platelets (supplemental Figure V). This finding strongly supports the notion that attenuated oxidative stress in $Agtr1^{-/-}$ platelets is, at least in part, responsible for the impaired platelet aggregation.

Platelet AT_1 Receptor Deficiency Inhibits the Expression and Release of SDF-1α

Immunohistochemical analysis revealed that the number of $CD41^+SDF\text{-}1\alpha^+$ platelets was markedly increased (3.2-fold) in the $Agtr1^{+/+}$ platelets after thrombin stimulation, whereas it was severely inhibited (1.8-fold) in $Agtr1^{-/-}$ platelets (Figure 5A). Furthermore, the SDF-1α protein in the conditioned medium after thrombin stimulation was significantly reduced in $Agtr1^{-/-}$ platelets compared with $Agtr1^{+/+}$ platelets (Figure 5B), suggesting that impaired platelets aggregation contributed to the decreased serum level of SDF-1α.

Discussion

The present study provides new evidence that deficiency of the BM-AT_1 receptor inhibits neointimal formation after vascular injury by affecting the mobilization and homing of BM-derived VPCs (rather than EPCs) in a SDF-1α–dependent manner. Platelet-derived SDF-1α at the sites of injury and the serum level of SDF-1α were profoundly impaired in chimeric mice with Agtr1$^{-/-}$ BM cells, followed by the reduction of both circulating VPCs and vascular VPCs incorporated into neointima. Inhibition of platelet aggregation by ADP receptor blocker ticlopidine markedly suppressed platelet-derived SDF-1α production, which resulted in a decrease in circulating VPCs and attenuation of neointima formation (supplemental Figure VI). These findings provide a new insight into the action of BM-AT_1 on the mobilization and homing kinetics of BM-derived vascular-lineage progenitors in the vascular repair.

The SDF-1α/CXCR4 axis has been shown to be implicated in the mobilization and homing of EPCs as well as VPCs.[7] Stellos et al[18] reported that platelet-derived SDF-1α enhanced the accumulation of CD34$^+$ cells at sites of injury after intravenously injection of CD34$^+$ cells. Likewise, Xiao et al[2] reported that local transplantation of embryonic stem cell–derived EPCs inhibited neointimal hyperplasia after wire-induced femoral arterial injury. However, the direct effect of platelet-derived SDF-1α on the mobilization and homing of EPCs was not investigated in these experiments. Zernecke et al[4] showed that blocking of SDF-1α after injury reduced the percentage of gated events of VPCs rather than those of EPCs. Taken together, SDF-1α appears to be preferentially involved in the mobilization and homing of VPCs rather than EPCs in the pathogenesis of neointima formation after vascular injury.

The effect of AT_1 blockade on the kinetics of BM-derived VPCs after vascular injury remains poorly understood. Yamada et al[13] recently investigated the effect of ARB on the homing of BM-derived smooth muscle–like cells using BM chimeric mice whose BM was repopulated with apoE$^{-/-}$/GFP$^+$ cells. ARB treatment has been shown to reduce vascular oxidative stress and the redox-sensitive gene expression of chemokines and other inflammation-promoting factors,[9,10] all of which are critically involved in the mobilization and homing of BM-derived VPCs. In this study, BM chimeric mice were newly generated, which enabled the investigation of AT_1-mediated effects on BM-derived progenitor cells independently of vascular AT_1-mediated actions. Although the number of BM-VPCs did not differ between BM-Agtr1$^{-/-}$ and BM-Agtr1$^{+/+}$ mice, circulating VPCs after injury were markedly reduced in BM-Agtr1$^{-/-}$ mice. This finding suggests that the mobilization of VPCs after vascular injury was impaired by BM-AT_1 deficiency independent of vascular AT_1-mediated actions. Ohtani et al[12] found that trasnsdifferentiation of peripheral blood MNCs to smooth muscle progenitor cells was severely suppressed in ARB-treated animals, consistent with our present observation that ARB treatment significantly reduced the number of circulating VPCs after injury (supplemental Figure VII). Considering that platelet-derived SDF-1α causes the homing of BM-derived progenitor cells into injured arteries,[15] these findings suggest for the first time that AT_1 blockade attenuates the mobilization and homing of BM-derived VPCs into neointima by inhibiting platelet aggregation and the production of vascular SDF-1α without any effect on EPC-mediated reendothelialization.

Harada et al[19] previously reported that neointima formation after vascular injury was not suppressed in AT_1-deficient mice compared with wild-type mice, and they also described the possibility that growth factors and vasoactive peptides, such as FGF-2, PDGF-B, TGF-β1, and endotheline-1, etc, might substitute fully for AT_1-mediated actions in AT_1-deficient mice.[19] We therefore compared the expression levels of FGF-2, PDGF-B, and TGF-β1 mRNAs between wild-type and AT_1-deficient mice. We found that the relative expression levels of FGF-2 and PDGF-B mRNAs in the injured vessels were actually higher in AT_1-deficient mice than wild-type mice, whereas TGF-β1 mRNA levels were equivalent between the 2 groups (supplemental Figure VIII). FGF-2 mRNA expression in BM-Agtr1$^{-/-}$ mice was also significantly higher than BM-Agtr1$^{+/+}$ mice, however the extent was much lower than AT_1-deficient mice. The mRNA expression levels of PDGF-B and TGF-β1 did not show any difference between BM-Agtr1$^{+/+}$ and BM-Agtr1$^{-/-}$ mice. These findings confirm the involvement of growth factors in neointima formation after vascular injury in AT_1-deficient mice, and provide evidence that BM-AT_1 rather than vascular AT_1 plays a more important role in the formation of neointima.

AT_2 receptor has also been reported to play a crucial role in neointima formation after vascular injury,[11] therefore we newly generated bone marrow chimeric mice whose bone marrow cells were repopulated with Agtr2$^{+/+}$ (BM-Agtr2$^{+/+}$) or Agtr2$^{-/-}$ (BM-Agtr2$^{-/-}$) cells. In contrast to the effect of BM-AT_1, neointimal area and neointima/media ratio were significantly increased by 40% and 39% in BM-Agtr2$^{-/-}$ mice compared with BM-Agtr2$^{+/+}$ mice (supplemental Figure IXA and IXB), which was consistent with the previous findings that neointimal hyperplasia was exaggerated in Agtr2$^{-/-}$ mice.[11] Reendothelialization and the numbers of VPCs did not differ between BM-Agtr2$^{+/+}$ and BM-Agtr2$^{-/-}$ mice (supplemental Figures IXC, IXD, and X). Similarly, the extent of aggregated platelets and their colocalization with SDF-1α showed no discernable difference between the two groups of mice (supplemental Figure XI). In agreement with these findings, serum concentrations of SDF-1α 3 days after injury and the number of Sca-1$^+$CD31$^-$ cells incorporating into the injured artery in BM-Agtr2$^{-/-}$ mice were equivalent with those in BM-Agtr2$^{+/+}$ mice (supplemental Figure XII). These findings suggest that BM-AT_2 receptor counteracts the effect of BM-AT_1 on the development of neointimal formation, however underlying mechanisms for BM-AT_2-mediated vasoprotective actions are different from those of BM-AT_1, and further studies will be required to clarify it.

We also studied the effects of BM-AT_1 and BM-AT_2 on apoptosis in the development of neointimal formation. The

TUNEL index, which was calculated as the ratio of TUNEL-positive nuclei to total nuclei in the neointima and media, showed a slightly increase in BM-Agtr1$^{-/-}$ mice, whereas it was modestly, but not significantly, reduced in BM-Agtr2$^{-/-}$ mice compared with control mice (supplemental Figure XIII). Because all of the cells in neointima and media are not derived from bone marrow, the effects of BM-AT_1 or BM-AT_2 on apoptosis might be modest compared with the previous study in which total cells are AT_1-deficient or AT_2-deficient cells.[11]

This study provides novel important evidence that BM-AT_1 contributes to neointima formation after vascular injury by promoting the mobilization and homing of BM-derived VPCs in a platelet-derived SDF-1α–dependent manner, and that AT_1 deficiency inhibits SDF-1α release by blocking aggregation of platelets. Such relationship between BM vascular-lineage progenitors and BM renin-angiotensin system, especially in terms of platelet-SDF-1α/VPCs interaction, may provide a new insight into the role of renin–angiotensin system in the pathogenesis of vascular repair.

Acknowledgments

We thank Prof T. Todo and J. Kobayashi, and the Radiation Biology Center Kyoto University (H18-17) for assistance with bone marrow transplantation.

Sources of Funding

This work was supported by a grant from the Ministry of Education, Culture, Sports, Science and Technology of Japan (00240036).

Disclosures

None.

References

1. Inoue T, Sata M, Hikichi Y, Sohma R, Fukuda D, Uchida T, Shimizu M, Komoda H, Node K. Mobilization of CD34-positive bone marrow-derived cells after coronary stent implantation: Impact on restenosis. *Circulation.* 2007;115:553–561.
2. Xiao Q, Zeng L, Zhang Z, Margaruti A, Ali ZA, Channon KM, Xu Q, Hu Y. Sca-1$^+$ progenitors derived from embryonic stem cells differentiation into endothelial cells capable of vascular repair after arterial injury. *Arterioscler Thromb Vasc Biol.* 2006;26:2244–2251.
3. Schober A, Knarren S, Lietz M, Lin EA, Weber C. Crucial role of stromal cell-derived factor-1α in neointima formation after vascular injury in apolipoprotein E-deficient mice. *Circulation.* 2003;108:2491–2497.
4. Zernecke A, Schober A, Bot I, Hundelshausen P, Liehn EA, Möpps B, Mericskay M, Gierschik P, Biessen EA, Weber C. SDF-1α/CXCR4 axis is instrumental in neointimal hyperplasia and recruitment of smooth muscle progenitor cells. *Circ Res.* 2005;96:784–791.
5. Shiba Y, Takahashi M, Yoshioka T, Yajima N, Morimoto H, Izawa A, Ise H, Hatake K, Motoyoshi K, Ikeda U. M-CSF accelerates neointimal formation in the early phase after vascular injury in mice: The critical role of the SDF-1-CXCR4 system. *Arterioscler Thromb Vasc Biol.* 2007;27:283–289.
6. Sakihara H, Masunaga T, Yamashita K, Hashimoto T, Inobe M, Todo S, Uede T. Stromal cell-derived factor-1 and CXCR4 interaction is critical for development of transplant arteriosclerosis. *Circulation.* 2004;110:2924–2930.
7. Walter DH, Haendeler J, Reinhold J, Rochwalsky U, Seeger F, Honold J, Hoffmann J, Urbich C, Lehmann R, Arenza-Seisdesdos F, Aicher A, Heeschen C, Fichtlscherer S, Zeiher AM, Dimmeler S. Impaired CXCR4 signaling contributes to the reduced neovascularization capacity of endothelial progenitor cells from patients with coronary artery disease. *Circ Res.* 2005;97:1142–1151.
8. Zhang LN, Wilson DW, Cunha V, Sullivan ME, Vergona R, Rutledge JC, Wang YX. Endothelial NO synthase deficiency promotes smooth muscle progenitor cells in association with upregulation of stromal cell-derived factor -1α in a mouse model of carotid artery ligation. *Arterioscler Thromb Vasc Biol.* 2006;26:765–772.
9. Paul M, Mehr AP, Kreutz R. Physiology of local renin-angiotensin systems. *Physiol Rev.* 2006;86:747–803.
10. Mehta PK, Griendling KK. Angiotensin II cell signaling: physiological and pathological effects in the cardiovascular system. *Am J Physiol Cell Physiol.* 2007;292:C82–C97.
11. Suzuki J, Iwai M, Nakagami H, Wu L, Chen R, Sugaya T, Hamada M, Hiwada K, Horiuchi M. Role of angiotensin II-regulated apoptosis through distinct AT_1 and AT_2 receptors in neointimal formation. *Circulation.* 2002;106:847–853.
12. Ohtani K, Egashira K, Ihara Y, Naoko K, Funakoshi K, Zhao G, Sata M, Sunagawa K. Angiotensin II type 1 receptor blockade attenuates in-stent restenosis by inhibiting inflammation and progenitor cells. *Hypertension.* 2006;48:664–670.
13. Yamada T, Kondo T, Numaguchi Y, Tsuzuki M, Matsubara T, Manabe I, Sata M, Nagai R, Murohara T. Angiotensin II receptor blocker inhibits neointimal hyperplasia through regulation of smooth muscle-like progenitor cells. *Arterioscler Thromb Vasc Biol.* 2007;27:2363–2369.
14. Peter S, Trummel M, Meyners W, Koehler B, Westermann K. Valsartan versus ACE inhibition after bare metal stent implantation-results of the VALVACE trial. *Int J Cardiol.* 2005;98:331–335.
15. Massberg S, Konrad I, Schürzinger K, Lorenz M, Schneider S, Zohlnhoefer D, Hoppe K, Schiemann M, Kennerknecht E, Sauer S, Schulz C, Kerstan S, Rudelius M, Seidl S, Sorge F, Langer H, Peluso M, Goyal P, Vestweber D, Emambokus NR, Busch DH, Frampton J, Gawaz M. Platelets secrete stromal cell-derived factor 1α and recruit bone marrow-derived progenitor cells to arterial thrombi in vivo. *J Exp Med.* 2006;203:1221–1233.
16. Kalinowski L, Matys T, Chabielska E, Buczko W, Malinski T. Angiotensin II AT1 receptor antagonists inhibit platelet adhesion and aggregation by nitric oxide release. *Hypertension.* 2002;40:521–527.
17. Freedman JE. Translational therapeutics at the platelet vascular interface: Oxidative stress and platelets. *Arterioscler Thromb Vasc Biol.* 2008;28:s11–s16.
18. Stellos K, Langer H, Daub K, Schoenberger T, Gauss A, Geisler T, Bigalke B, Mueller I, Schumm M, Schaefer I, Seizer P, Kraemer BF, Siegel-Axel D, May AE, Lindemann S, Gawaz M. Platelet-derived stromal cell-derived factor-1 regulates adhesion and promotes differentiation of human CD34$^+$ cells to endothelial progenitor cells. *Circulation.* 2008;117:206–215.
19. Harada K, Komuro I, Sugaya T, Murakami K, Yazaki Y. Vascular injury causes neointimal formation in angiotensin II type 1a receptor knockout mice. *Circ Res.* 1999;84:179–185.

Combined Effects of Bisphosphonate and Radiation on Osteosarcoma Cells

KAZUTERU RYU[1], HIROAKI MURATA[1], KAZUTAKA KOTO[1], NAOYUKI HORIE[1], TAKAAKI MATSUI[1], YASUNORI NISHIGAKI[1], TOMOYA SAKABE[1], HIDEYUKI TAKESHITA[1], MEGUMI ITOI[1], SHINYA KIMURA[2], EISHI ASHIHARA[3], TAIRA MAEKAWA[3], SHINJI FUSHIKI[4] and TOSHIKAZU KUBO[1]

[1]Department of Orthopaedics, and [4]Department of Pathology and Applied Neurobiology, Graduate School of Medical Science, Kyoto Prefectural University of Medicine, 465 Kawaramachi-Hirokoji, Kamigyo-ku, Kyoto 602-8566, Japan;
[2]Division of Hematology, Respiratory Medicine, and Oncology, Department of Internal Medicine, Faculty of Medicine, Saga University, 5-1-1 Nabeshima, Saga 849-8501, Japan;
[3]Department of Transfusion Medicine and Cell Therapy, Kyoto University Hospital, 54 Kawahara-cho Shogoin, Sakyo-ku, Kyoto 606-8507, Japan;

Abstract. *Antitumour effects of third-generation bisphosphonates (BPs), such as zoledronic acid (ZOL), and the combined effects of ZOL with other anticancer agents against osteosarcoma cells have been reported previously. The aim of this study was to identify further combined antitumour effects using BPs and radiation in osteosarcoma cell lines. Materials and Methods: Cell proliferation, cell cycle analysis, and nuclear morphology were examined in each osteosarcoma cell line divided into three groups (ZOL alone, radiation alone and the ZOL/radiation combination). Results: Combined therapy (low-concentration ZOL and low-dose radiation) had significant growth inhibitory effects compared to the use of ZOL or radiation individually. Flow cytometric analysis revealed an increase in cells in the sub-G_1 phase by combined treatment, and apoptotic cells were also observed. Conclusion: These findings suggest that combination therapy using BPs and radiation may be a promising therapy for osteosarcoma, producing fewer side effects and complications in the near future.*

Osteosarcoma is a high-grade malignant bone neoplasm that commonly occurs in juvenile patients. Although the prognosis of these patients has improved substantially through the development of effective adjuvant or neoadjuvant regimens of chemotherapy, >20% patients still die as a result of tumour metastasis and unresectable tumour (1-5).

Chemotherapy for bone and soft tissue tumours is problematic since high-dose drugs are required compared with other tumour types due to the low concentration of drug reaching the tissue, and serious adverse drug reactions often oblige chemotherapy to be halted in patients such as those with elderly onset tumours. Therefore, new antitumour drugs and new therapy methods are urgently needed for bone and soft tissue tumours. Various new osteosarcoma therapies have been investigated worldwide, with many clinical trials performed on novel agents. Among these agents, the antitumour effects of bisphosphonates (BPs) have been recently reported (6-8).

BPs are effective inhibitors of bone resorption and have been used for the past three decades in the treatment of metabolic bone diseases (9). BPs can be divided into two classes based on differences in the structure of the R2 side-chain. Nitrogen-containing BPs (N-BPs), or so-called second- and third-generation BPs, have a basic nitrogen-containing moiety in the R2 side-chain. Non-nitrogen-containing BPs (Non N-BPs), or so-called first-generation BPs, do not contain a nitrogen in the R2 side-chain and are less potent antiresorptive agents than N-BPs.

N-BPs induce apoptosis in osteoclasts by inhibiting protein prenylation in small G-proteins through inhibition of farnesyl pyrophosphate synthase in the mevalonate pathway (10).

It has previously been reported that third-generation BPs, such as zoledronic acid (ZOL) and minodronic acid (YM529), show direct antitumour effects and synergistically augment the effects of anticancer agents in various cancer cell lines (11-15). Recently, several investigators have

Correspondence to: Hiroaki Murata, MD, Ph.D., Department of Orthopaedics, Graduate School of Medical Science, Kyoto Prefectural University of Medicine, 465 Kawaramachi-Hirokoji, Kamigyo-ku, Kyoto 602-8566, Japan. Tel: +81 752515549, Fax: +81 752515841, e-mail: murah@koto.kpu-m.ac.jp

Key Words: Osteosarcoma, bisphosphonate, radiation, combined effects.

reported the anti-osteosarcoma effects of third-generation BPs *in vitro* (16-21) and *in vivo* (22-24).

In addition, the antitumour effects and the mechanism of third-generation BPs have previously been reported in murine osteosarcoma cell lines *in vitro* in order to clarify the direct anti-bone tumour effects of BPs. As a result, third-generation BPs halted the cell cycle at the S-phase, leading osteosarcoma cells to apoptosis (20).

However, BPs cannot overcome drug resistance alone; therefore, combination therapy with various antitumour drugs and third-generation BPs has been investigated (21). Those data revealed that BPs inhibit the growth of murine osteosarcoma cell lines by combination therapy compared with individual therapies.

Another well-established treatment modality for the local treatment of bone metastases is radiotherapy. Combined chemotherapy and radiotherapy for osteosarcoma has already been used clinically (25). Likewise, combined therapy using ZOL and radiotherapy may further inhibit cell growth, thereby decreasing the drug concentration and amount of irradiation to ultimately be safer than when used alone, with lower side effects.

Recently, there have been several reports concerning the combined effects of third-generation BPs with radiation in various cancer cell lines; for example breast cancer (26), prostate cancer, myeloma (27), lung cancer (28). However, there is no report on the combined effect of ZOL with radiation in osteosarcoma cells. Therefore, this study aimed to clarify the combined effect of BPs and radiation, and to analyse the cell cycle and induction of apoptosis in osteosarcoma cells.

Materials and Methods

Reagents. ZOL, (1-hydroxy-2-(1H-imidazole-1-yl) ethylidene-bisphosphonic acid, was obtained from Novartis Pharma AG (Basel, Switzerland). ZOL was dissolved in Ca^+ Mg^+ phosphate-buffered saline (PBS) and stored at –20°C. Appropriate drug concentrations were made by dilution with fresh medium immediately before each experiment.

X-Ray irradiation. Cultured cells were irradiated with 150-400cGy X-Ray using SOFTEX M-150WE (SOFTEX CO, LTD, Tokyo, Japan). The irradiation conditions selected were a distance of 1 cm from the focus to the specimen, an irradiation rate of 0.5 Gy/min in air.

Cell lines. A murine osteosarcoma cell line, LM8, was established from the murine Dunn osteosarcoma cell line (29). The MOS cell line was established from the murine osteosarcoma model developed at Massachusetts General Hospital (30). MG-63 was used as human osteosarcoma cells (31). These cells were maintained in Dulbecco's modified Eagle's medium supplemented with 15 mM HEPES buffer, 10% foetal bovine serum, and antibiotic solutions of penicillin (100 U ml^{-1}) and streptomycin (100 μg ml^{-1}). All cells were cultured at 37°C in a fully humidified incubator with 5% CO_2. All experiments described were performed at least three times using cells in the exponential growth phase.

Concurrent exposure to ZOL and radiation MTT assay. Proliferation of the cell lines was determined using the methyl-thiazol-diphenyl-tetrazolium (MTT) assay, as previously described (32). LM8, MOS and MG-63 cells were cultivated in a flat-bottomed 96-well plate (Greiner Labortechnik, Frickenhausen, Germany) at 1×10^4 cells per well in 100 μl medium and incubated for 24 h, followed by incubation with various concentrations of ZOL and/or radiation at various doses for a further 72 h. The means of six data values for each treatment were calculated. For all cell lines, the linear relationship between the degree of proliferation and cell number was evaluated within the range of the experiment. Half-maximal inhibitory concentrations (IC_{50}s) were determined and, based on the IC_{50}s, the combined effects of ZOL at lower concentrations than IC_{50} with radiation at a lower dose than IC_{50} were investigated. LM8, MOS and MG-63 cells were treated with various lower concentrations of ZOL combined with various lower doses of radiation for 72 h. After 72 h, the rate of growth inhibition was evaluated by MTT assay. Data from three independent experiments were collected and Student's *t*-test was used to evaluate the efficacy of sequential treatment of ZOL and to compare the effects of each radiation alone or combination. *P*-values <0.05 were considered statistically significant and were derived from two-sided statistical tests.

Cell cycle analysis. To explore the possible mechanisms of ZOL alone, radiation alone or the combined effects of ZOL and radiation, LM8 cells were cultivated in a flat-bottomed 6-well plate at 2×10^4 cells/ml and analysed for cell cycle alterations by staining with propidium iodide (Sigma Aldrich, St. Louis, USA) after exposure to ZOL and/or radiation at various doses for 24 h, as previously described (33). The stained nuclei were analysed using a FACSCalibur flow cytometer (Becton Dickinson, Franklin Lakes, USA). DNA histograms were created using Cell Quest™ software for Apple Macintosh (Becton Dickinson).

Analysis of nuclear morphology. LM8 cells treated with ZOL and radiation under appropriate conditions were cultured for 72 h, fixed with 2% paraformaldehyde in PBS for 10 min, and then stained with DAPI (4',6-diamidino-2-phenylindole dihydrochloride) (Nacalai Tesque, Inc, Kyoto, Japan) at 4°C in the dark. For fluorescence microscopy, cells were cytospun onto slides and examined using a universal microscope (Nikon, Tokyo, Japan) with UV illumination. Apoptotic cells were identified on the basis of characteristic changes, including nuclear condensation, fragmentation, and apoptotic bodies.

Results

Growth inhibitory effects of ZOL against murine and human osteosarcoma cells. ZOL inhibited the growth of murine and human osteosarcoma cells (LM8, MOS, MG-63) dose dependently. The IC_{50} values of ZOL for LM8, MOS, MG-63 after 72 h exposure were 8.5, 2.4 and 27 μM, respectively, as shown in Figure 1. ZOL effectively inhibited osteosarcoma

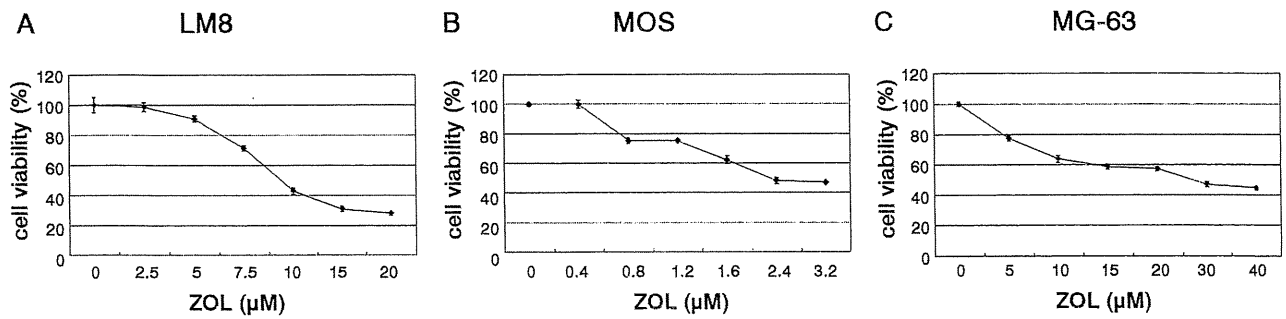

Figure 1. *Growth inhibitory effect of ZOL. The ability of ZOL to inhibit the growth of LM8 (A), MOS (B) and MG-63(C) cells was determined by MTT assay, respectively. Data are presented as the mean±s.d. of three independent experiments.*

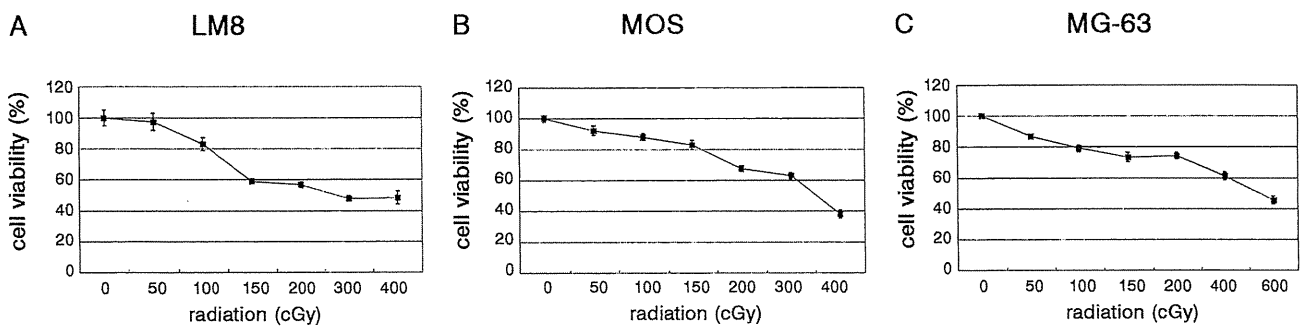

Figure 2. *Growth inhibitory effect of radiation. The ability of radiation to inhibit the growth of LM8 (A), MOS (B) and MG-63 (C) cells was determined by MTT assay, respectively. Data are presented as the mean±s.d. of three independent experiments.*

cell growth; however, the IC_{50} of ZOL of the human osteosarcoma cell line was higher than that of murine osteosarcoma cell lines.

Growth inhibitory effects of radiation against murine and human osteosarcoma cells. Radiation inhibited the growth of murine and human osteosarcoma cells, dose dependently. As shown in Figure 2, the IC_{50} values of ZOL for LM8, MOS, MG-63 after 72 h exposure were 300, 360 and 530cGy, respectively. The irradiation amount at IC_{50} for MG-63 cells, the human osteosarcoma cell line, was higher than for LM8 or MOS cells, murine osteosarcoma cell lines. Radiation showed almost the same antitumour activity for human and murine osteosarcoma cell lines.

Growth inhibitory effects of combination therapy against murine and human osteosarcoma cells. The combined effects of ZOL at lower concentrations with radiation at lower doses than IC_{50} for murine and human osteosarcoma cells, LM8, MOS and MG-63 were examined. The combined use of lower doses of ZOL and radiation induced significantly higher antitumour effects than when used alone, as shown in Figure 3. A significant growth inhibitory effect of combination with ZOL at higher than 5 μM under all irradiation conditions against LM8 cells was observed. ZOL 5 μM with irradiation at 100cGy inhibited the growth of LM8 cells to the IC_{50} level. In particular, the antitumour effect when treated with 7.5 μM ZOL combined with 150 cGy irradiation was stronger than when treated alone. Concerning MOS cells, no significant difference was observed in the combination of ZOL at 0.4 μM with irradiation at 50 cGy. A significant growth inhibitory effect was observed with ZOL at higher than 0.8 μM and irradiation at higher than 100 cGy. Cell growth could be inhibited to the IC_{50} level by the combination of ZOL at 1.2 μM with irradiation at 150 cGy. In Figure 3C, a significant growth inhibitory effect was observed under all conditions against MG-63 cells. The combination of ZOL with radiation strongly inhibited cell viability in each cell line compared to when used alone, even if at a higher concentration or higher irradiation amount.

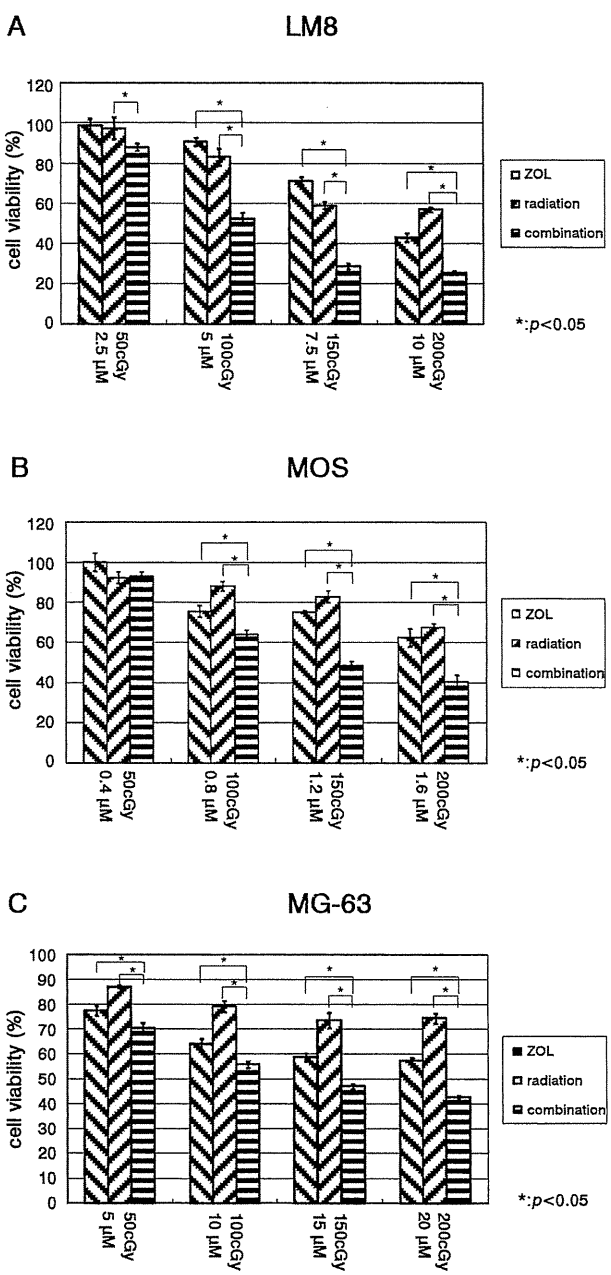

Figure 3. *Growth inhibitory effect of combination. The ability of combination to inhibit the growth of LM8 (A), MOS (B) and MG-63 (C) cells was determined by MTT assay, respectively. Data are presented as the mean±s.d. of three independent experiments.*

Combined effects of ZOL with radiation on the alterations of cell cycle. When LM8 cells were treated with 7.5 μM ZOL combined with 150 cGy radiation for 72 h, there was an increase of cells in the S-phase between G_0/G_1 and G_2M-phases and in the rate of LM8 cells in sub-G_1 compared with ZOL and radiation alone (Figure 4A). Three patterns for the proportions of the cell in the sub-G_1 are shown in Figure 4B. When LM8 cells were treated with ZOL 7.5 μM with irradiation of 150 cGy, many cells in the sub-G_1 increased in contrast to other conditions.

Combined effects of ZOL with radiation on nuclear morphology. When LM8 cells were treated with 7.5 μM ZOL combined with 150 cGy radiation for 72 h and stained with DAPI, the nuclear fragmentation and apoptotic bodies characteristic of apoptosis were observed (Figure 5).

Discussion

BPs are widely used to treat bone diseases, such as osteoporosis and metastatic bone tumours. Recently, there have been reports on their antitumour effect. The mechanisms of the antitumour effects of BPs are thought to be 'BP triangle' effects, *i.e.* the integration of the following three factors: changes in the bone marrow micro-environment with apoptosis of osteoclasts, immunological mechanism through γδT-cells induced by N-BPs, and direct antitumour effects by inhibiting protein prenylation in small G-proteins (34). It has been shown that BPs provide useful information on various malignant tumours according to previous reports; however, one of the problems in clinical use is that the IC_{50} is high, because BPs are rapidly cleared from the circulation within a few hours (35-37).

Current trends in the treatment of human tumours are the combination of BPs with anticancer agents. This approach results in improved responses as well as the ability to use lower and less toxic concentrations of the drugs. Other investigators have demonstrated the synergistic or additive growth inhibition of ZOL and various antitumour drugs against leukemia (11, 12), lung cancer (13), bladder cancer (35), and breast cancer (36, 37). It has also been demonstrated that the combination of ZOL with doxorubicin, cisplatin, paclitaxel or gemcitabine may be effective against murine osteosarcoma cells, compared to any of these agents alone (21).

On the other hand, there are several reports concerning the combined effects of third-generation BPs with radiation in various cancer cell lines, for example breast cancer (26), prostate cancer, myeloma (27) and lung cancer (28) to obtain further antitumour effects. The IC_{50} of MCF-7, a human breast cancer cell line, was 20 μM by ZOL alone, 500 cGy by irradiation alone, and 10 μM and 200 cGy for the combination of ZOL with irradiation (26). According to Algur *et al.*, the IC_{50} of C4-2, a human prostate cancer cell line, was 82 μM with ZOL alone, 1314.6 cGy with irradiation alone, and 32 μM and 320.4 cGy for the combination of ZOL with irradiation ZOL (27). In this report, it was shown that the combination of ZOL with radiation showed true synergism, rather than when used alone, as shown clearly by the growth

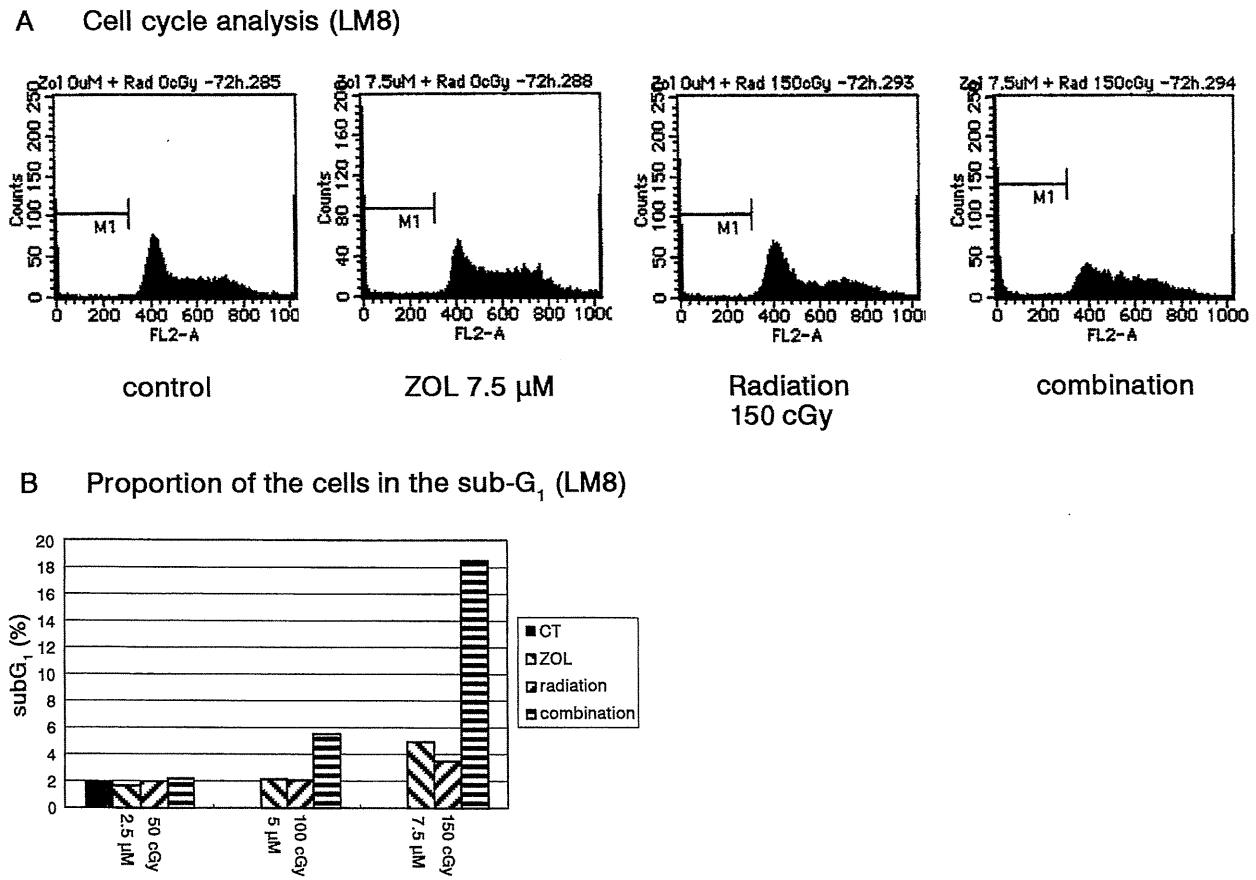

Figure 4. *Cell cycle analysis and proportion of the cell in the sub-G_1. A: Cell cycle analysis of combined treatment of ZOL with radiation. The effect of agents on the cell cycle was evaluated by flow cytometry of osteosarcoma cells that had been exposed to 7.5 μM ZOL combined with 150 cGy radiation for 72 h. B: There was a significant increase in the ratio of LM8 cells in sub-G_1 compared with ZOL (at 5 μM or 7.5 μM) or radiation (at 100 cGy and 150 cGy) alone.*

inhibitory effects against murine and human osteosarcoma cells (Figure 3). Stronger combination effects were observed in MG-63 than prostate cancer and were equal to breast cancer. In this study, it was reported that the combined use of lower doses of ZOL and radiation enhanced the antitumour effects than when used alone in murine and human osteosarcoma cells, LM8, MOS and MG-63, through an increase in the ratio of cells in sub-G_1, growth inhibition, and apoptosis induced by nuclear fragmentation. Thus, combination therapy using BPs and radiotherapy may be useful to increase the antitumour effects and to decrease side-effects and complications. According to previous reports, the IC_{50} of ZOL in osteosarcoma cell lines is lower than in other cancer cell lines; therefore, treatment of osteosarcoma with a lower concentration of ZOL is achievable clinically. These results of the combination of BPs and radiation are novel and intriguing, suggesting the clinical utility of using BPs combined with radiation, especially in patients with osteosarcoma.

However, the precise synergistic mechanism of ZOL and radiation is currently unknown. The biochemical mechanism of action of BPs is now well documented, with N-BPs such as ZOL affecting cellular behavior through inhibition of the mevalonate pathway (9). In a previous paper, the potential mechanisms of the antiproliferative effect of ZOL, which include direct apoptosis induction, and indirect anticancer effects were reviewed (34).

Radiotherapy is one of the most effective treatments for bone metastases (38-41). Generally, tumour cells are usually most sensitive during the latter part of the S-phase and in the G_2- or M-phase for radiotherapy (42). Ural *et al.* reported by flow cytometric analysis of ZOL-treated multiple myeloma cells an increase in the proportion of cells in the S-phase, possibly due to slower progression through the S-phase or a block between the S-phase and G_2M-phase in the cell cycle (26, 43). Using a small cell lung cancer cell line, Matsumoto *et al.* reported that cell growth inhibition may involve not only the induction of

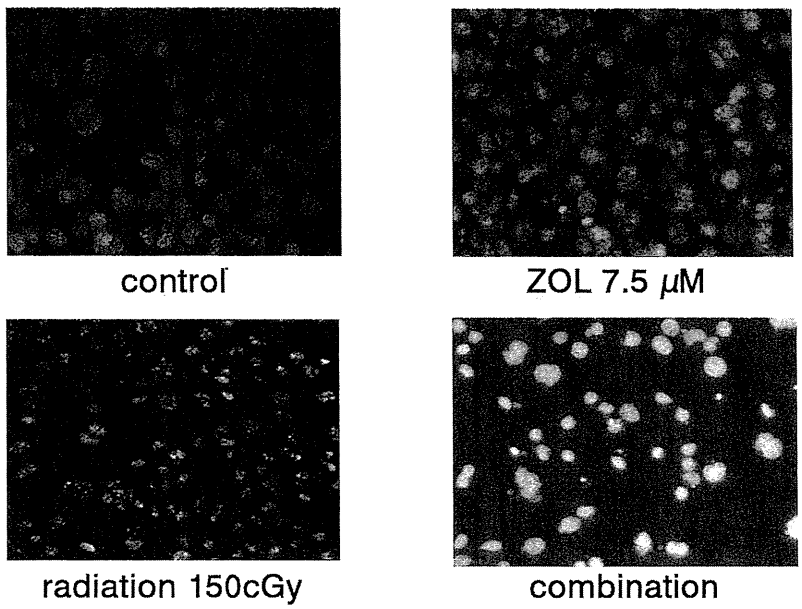

Figure 5. *DAPI staining (LM8). Untreated LM8 cells or LM8 cells treated with 7.5 μM ZOL, 150 cGy radiation, and combined with both for 72 h were stained with DAPI.*

apoptosis, but also the prolongation of cell cycle progression by ZOL alone or combined with anticancer agents (13). This ability of ZOL to arrest cells in the G_2M-phase or to prolong cell cycle progression raises the possibility of ZOL as a potential cell cycle radiosensitizer because G_2 and M cells are more sensitive than cells within other cell cycle phases (44).

In the present study, the mechanism of the combined effects of ZOL and radiation was investigated using flow cytometry in order to gain further insights into their mechanism of action for osteosarcoma. There was no alteration of the cell cycle by ZOL alone or by radiation alone when we investigated at lower doses of ZOL or radiation than IC_{50}; however, when a lower dose of ZOL was combined with a lower dose of radiation, cells in the S-phase increased, despite the fact that ZOL or radiation used individually did not affect the cell cycle. Moreover, when ZOL with radiation showed a strong antitumour effect against osteosarcoma cells, combined therapy induced not only an increase of sub-G_1 cells but also the appearance of apoptotic cells. These results indicated that ZOL and radiation might cause DNA damage and enhance cytotoxic activity together. Therefore, it is difficult to clarify the mechanism of the combined effect of ZOL and radiation although there have been some reports by flow cytometric analysis. Other factors should be considered other than the cell cycle.

In conclusion, the combined use of lower doses of ZOL and radiation enhanced the cytotoxic effects compared to their individual use in murine and human osteosarcoma cells. Combining lower radiation treatment with a lower dose of ZOL might produce the same effect as the standard ZOL and radiation dose, thus producing fewer side-effects and complications. This combination method may be a promising therapy for osteosarcoma in the near future.

Acknowledgements

This work was supported by KAKENHI (Grant-in-Aid for Scientific Research C:20591764 to HM)

References

1 Unni KK: Osteosarcoma. *In*: Dahlin's Bone Tumors: General Aspects and Data on 11087 Cases, 5th ed. Unni KK (ed.). Philadelphia, Lippincott-Raven, pp. 143-183, 1996.

2 Murayama T, Kawasoe Y, Yamashita Y, Ueno Y, Minami S, Yokouchi M and Komiya S: Efficacy of the third-generation bisphosphonate risedronate alone and in combination with anticancer drugs against osteosarcoma cell lines. Anticancer Res *28*: 2147-2154, 2008.

3 Nishi T, Kusumi T, Tanaka M, Sato F, Sasaki M, Kudo H and Kijima H: Establishment of transplantable murine osteosarcoma cell line with endochondral ossification. Anticancer Res *28*: 1627-1631, 2008.

4 Walters DK, Steinmann P, Langsam B, Schmutz S, Born W and Fuchs B: Identification of potential chemoresistance genes in osteosarcoma. Anticancer Res *28*: 673-679, 2008.

5 Mueller F, Fuchs B and Kaser-Hotz B: Comparative biology of human and canine osteosarcoma. Anticancer Res *27*: 155-164, 2007.

6 Li YY, Chang JW, Chou WC, Liaw CC, Wang HM, Huang JS, Wang CH and Yeh KY: Zoledronic acid is unable to induce apoptosis, but slows tumor growth and prolongs survival for non-small-cell lung cancers. Lung Cancer *59*: 180-191, 2008.

7 Guenther A, Gordon S, Tiemann M, Burger R, Bakker F, Green JR, Baum W, Roelofs AJ, Rogers MJ and Gramatzki M: The bisphosphonate zoledronic acid has antimyeloma activity *in vivo* by inhibition of protein prenylation. Int J Cancer *126*: 239-246, 2010.

8 Sewing L, Steinberg F, Schmidt H and Göke R: The bisphosphonate zoledronic acid inhibits the growth of HCT-116 colon carcinoma cells and induces tumor cell apoptosis. Apoptosis *13*: 782-789, 2008.

9 Russel RGG and Rogers MJ: Bisphosphonates: From the laboratory to the clinic and back again. Bone *25*: 97-106, 1999.

10 Green JR: Antitumor effects of bisphosphonates. Cancer *97*: 840-847, 2003.

11 Kuroda J, Kimura S, Segawa H, Kobayashi Y, Yoshikawa T, Urasaki Y, Ueda T, Enjo F, Tokuda H, Ottmann OG and Maekawa T: The third-generation bisphosphonate zoledronate synergistically augments the anti-Ph$^+$ leukemia activity of imatinib mesylate. Blood *102*: 2229-2235, 2003.

12 Kimura S, Kuroda J, Segawa H, Sato K, Nogawa M, Yuasa T, Ottmann OG and Maekawa T: Antiproliferative efficacy of the third-generation bisphosphonate, zoledronic acid, combined with other anticancer drugs in leukemic cell lines. Int J Hematol *79*: 37-43, 2004.

13 Matsumoto S, Kimura S, Segawa H, Kuroda J, Yuasa T, Sato K, Nogawa M, Tanaka F, Maekawa T and Wada H: Efficacy of the third-generation bisphosphonate, zoledronic acid alone and combined with anti-cancer agents against small cell lung cancer cell lines. Lung Cancer *47*: 31-39, 2005.

14 Segawa H, Kimura S, Kuroda J, Sato K, Nogawa M, Yuasa T, Yokota A, Hodohara K, Fujiyama Y and Maekawa T: The anti-leukemic efficacy of the third-generation bisphosphonate ONO5920/YM529. Leuk Res *29*: 451-457, 2005.

15 Yuasa T, Nogawa M, Kimura S, Yokota A, Sato K, Segawa H, Kuroda J and Maekawa T: A third-generation bisphosphonate, minodronic acid (YM529), augments the interferon alpha/beta-mediated inhibition of renal cell cancer cell growth both *in vitro* and *in vivo*. Clin Cancer Res *11*: 853-859, 2005.

16 Evdokiou A, Labrinidis A, Bouralexis S, Hay S and Findlay DM: Induction of cell death of human osteogenic sarcoma cells by zoledronic acid resembles anoikis. Bone *33*: 216-228, 2003.

17 Kubista B, Trieb K, Sevelda F, Toma C, Arrich F, Heffeter P, Elbling L, Sutterlüty H, Scotlandi K, Kotz R, Micksche M and Berger W: Anticancer effects of zoledronic acid against human osteosarcoma cells. J Orthop Res *24*: 1145-1152, 2006.

18 Kubo T, Shimose S, Matsuo T, Tanaka K, Yasunaga Y, Sakai A and Ochi M: Inhibitory effects of a new bisphosphonate, minodronate, on proliferation and invasion of a variety of malignant bone tumor cells. J Orthop Res *24*: 1138-1144, 2006.

19 Tenta R, Sourla A, Lembessis P and Koutsilieris M: Bone-related growth factors and zoledronic acid regulate the PTHrP/PTH.1 receptor bioregulation systems in MG-63 human osteosarcoma cells. Anticancer Res *26*: 283-291, 2006.

20 Horie N, Murata H, Nishigaki Y, Matsui T, Segawa H, Nogawa M, Yuasa T, Kimura S, Maekawa T, Fushiki S and Kubo T: The third-generation bisphosphonates inhibit proliferation of murine osteosarcoma cells with induction of apoptosis. Cancer Lett *238*: 111-118, 2006.

21 Horie N, Murata H, Kimura S, Takeshita H, Sakabe T, Matsui T, Maekawa T, Kubo T and Fushiki S: Combined effects of a third-generation bisphosphonate, zoledronic acid with other anticancer agents against murine osteosarcoma. Br J Cancer *96*: 255-261, 2007.

22 Heymann D, Ory B, Blanchard F, Heymann MF, Coipeau P, Charrier C, Couillaud S, Thiery JP, Gouin F and Redini F: Enhanced tumor regression and tissue repair when zoledronic acid is combined with ifosfamide in rat osteosarcoma. Bone *37*: 74-86, 2005.

23 Ory B, Heymann MF, Kamijo A, Gouin F, Heymann D and Redini F: Zoledronic acid suppresses lung metastases and prolongs overall survival of osteosarcoma-bearing mice. Cancer *104*: 2522-2529, 2005.

24 Koto K, Horie N, Kimura S, Murata H, Sakabe T, Matsui T, Watanabe M, Adachi S, Maekawa T, Fushiki S and Kubo T: Clinically relevant dose of zoledronic acid inhibits spontaneous lung metastasis in a murine osteosarcoma model. Cancer Lett *274*: 271-278, 2009.

25 Schwarz R, Bruland O, Cassoni A, Schomberg P and Bielack S: The role of radiotherapy in osteosarcoma. Cancer Treat Res *152*: 147-64, 2010.

26 Ural AU, Avcu F, Candir M, Guden M and Ozcan MA: *In vitro* synergistic cytoreductive effects of zoledronic acid and radiation on breast cancer cells. Breast Cancer Res *8*: R52, 2006.

27 Algur E, Macklis RM and Häfeli UO: Synergistic cytotoxic effects of zoledronic acid and radiation in human prostate cancer and myeloma cell lines. Int J Radiat Oncol Biol Phys *61*: 535-542, 2005.

28 Ural AU and Avcu F: Radiosensitizing effect of zoledronic acid in small cell lung cancer. Lung Cancer *50*: 271-272, 2005.

29 Asai T, Ueda T, Itoh K, Yoshioka K, Aoki Y, Mori S and Yoshikawa H: Establishment and characterization of a murine osteosarcoma cell line (LM8) with high metastatic potential to the lung. Int J Cancer *76*: 418-422, 1998.

30 Choi CH, Sedlacek RS and Suit HD: Radiation-induced osteogenic sarcoma of C3H mouse: effects of *Corynebacterium parvum* and WBI on its natural history and response to irradiation. Eur J Cancer *15*: 433-442, 1979.

31 Iizuka M, Ando K, Aruga T, Furusawa Y, Itsukaichi H, Fukutsu K, Nagasawa H and Moriya H: Effects of reoxygenation on repair of potentially lethal radiation damage in cultured MG-63 osteosarcoma cells. Radiat Res *147*: 179-184, 1997.

32 Hansen MB, Nielsen SE and Berg K: Re-examination and further development of a precise and rapid dye method for measuring cell growth/cell kill. J Immunol Methods *119*: 203-210, 1989.

33 Kimura S, Maekawa T, Hirakawa K, Murakami A and Abe T: Alterations of c-myc expression by antisense oligodeoxynucleotides enhance the induction of apoptosis in HL-60 cells. Cancer Res *55*: 1379-1384, 1995.

34 Yuasa T, Kimura S, Ashihara E, Habuchi T and Maekawa T: Zoledronic acid – a multiplicity of anticancer action. Current Med Chem *14*: 2126-2135, 2007.

35 Sato K, Yuasa T, Nogawa M, Kimura S, Segawa H, Yokota A and Maekawa T: A third-generation bisphosphonate, minodronic acid (YM529), successfully prevented the growth of bladder cancer *in vitro* and *in vivo*. Br J Cancer *95*: 1354-1361, 2006.

36 Neville-Webbe HL, Evans CA, Coleman RE and Holen I: Mechanisms of the synergistic interaction between the bisphosphonate zoledronic acid and the chemotherapy agent paclitaxel in breast cancer cells *in vitro*. Tumour Biol *27*: 92-103, 2006.

37 Jagdev SP, Coleman RE, Shipman CM, Rostami-H A and Croucher PI: The bisphosphonate, zoledronic acid, induces apoptosis of breast cancer cells: evidence for synergy with paclitaxel. Br J Cancer *84*: 1126-1134, 2001.

38 Falkmer U, Järhult J, Wersäll P and Cavallin-Ståhl E: A systematic overview of radiation therapy effects in skeletal metastases. Acta Oncol *42*: 620-633, 2003.

39 Kagan AR, Rose CM, Bedwinek JM, Blitzer PH, Brascho DJ, Brown AP, Coia LR, Earle JD, Janjan NA, Lowy RO, Pieters RS Jr, Rotman M and Leibel SA: Bone metastases. American college of radiology. ACR appropriateness criteria. Radiology *215*: 1077-1104, 2000.

40 Rose CM and Kagan AR: The final report of the expert panel for the radiation oncology bone metastasis work group of the American college of Radiology. Int J Radiat Oncol Biol Phys *40*: 1117-1124, 1998.

41 Chow E, Danjoux C, Wong R, Szumacher E, Franssen E, Fung K, Finkelstein J, Andersson L and Connolly R: Palliation of bone metastases: a survey of patterns of practice among Canadian raidiation oncologists. Radiother Oncol *56*: 305-314, 2000.

42 Sinclair WK: Cyclic X-ray responses in mammalian cells *in vitro*. Radiat Res *33*: 620-643, 1968.

43 Ural AU, Yilmaz MI, Avcu F, Pekel A, Zerman M, Nevruz O, Sengul A and Yalcin A: The bisphosphonate zoledronic acid induces cytotoxicity in human myeloma cell lines with enhancing effects of dexamethasone and thalidomide. Int J Hematol *78*: 443-449, 2003.

44 Milas L, Hunter NR, Mason KA, Kurdoglu B and Peters LJ: Enhancement of tumor radioresonse of a murine mammary carcinoma by paclitaxel. Cancer Res *54*: 3506-3510, 1994.

Received April 28, 2010
Revised May 20, 2010
Accepted May 25, 2010

Biochemical and Biophysical Research Communications 393 (2010) 498–503

Contents lists available at ScienceDirect

Biochemical and Biophysical Research Communications

journal homepage: www.elsevier.com/locate/ybbrc

Use of bicistronic vectors in combination with flow cytometry to screen for effective small interfering RNA target sequences

Naoka Kamio [a,b,1], Hideyo Hirai [a,b,*,1], Eishi Ashihara [a], Daniel G. Tenen [c,d], Taira Maekawa [a], Jiro Imanishi [b]

[a] Department of Transfusion Medicine and Cell Therapy, Kyoto University Hospital, 54 Kawahara-cho, Shogoin, Sakyo-ku, Kyoto 606-8507, Japan
[b] Department of Microbiology and Immunology, Kyoto Prefectural University of Medicine, 465 Kajii-cho, Kamigyo-ku, Kyoto 606-8566, Japan
[c] Harvard Stem Cell Institute, Harvard Medical School, Boston, MA 02115, USA
[d] Cancer Science Institute, National University of Singapore, Singapore 117456, Singapore

ARTICLE INFO

Article history:
Received 1 February 2010
Available online 10 February 2010

Keywords:
Bicistronic vector
Flow cytometry
siRNA
Green fluorescent protein

ABSTRACT

The efficacy and specificity of small interfering RNAs (siRNAs) are largely dependent on the siRNA sequence. Since only empirical strategies are currently available for predicting these parameters, simple and accurate methods for evaluating siRNAs are needed. To simplify such experiments, target genes are often tagged with reporters for easier readout. Here, we used a bicistronic vector expressing a target gene and green fluorescent protein (GFP) to create a system in which the effect of an siRNA sequence was reflected in the GFP expression level. Cells were transduced with the bicistronic vector, expression vectors for siRNA and red fluorescent protein (RFP). Flow cytometric analysis of the transduced cells revealed that siRNAs for the target gene silenced GFP from the bicistronic vector, but did not silence GFP transcribed without the target gene sequence. In addition, the mean fluorescence intensities of GFP on RFP-expressing cells correlated well with the target gene mRNA and protein levels. These results suggest that this flow cytometry-based method enables us to quantitatively evaluate the efficacy and specificity of siRNAs. Because of its simplicity and effectiveness, this method will facilitate the screening of effective siRNA target sequences, even in high-throughput applications.

Introduction

RNA interference is a sequence-specific posttranscriptional gene-silencing process induced by short double-stranded RNA [1,2]. This evolutionally conserved phenomenon is widely applied to the functional analysis of genes and to therapeutic trials [3–7]. The specificity and efficacy of gene silencing with short interfering RNAs (siRNA) are largely dependent on the siRNA sequence. Accumulating evidence suggests that only a limited number of siRNAs are capable of inducing highly effective target gene silencing in a sequence-specific manner [8–11]. Many algorithms and guidelines have been developed for the design of effective siRNA sequences [12–16]. However, predicting siRNA efficacy and specificity remains empirical and requires experimental verification. Therefore, simple and accurate methods for evaluating siRNAs are required.

To directly measure the protein or mRNA levels of a target gene, gene-specific reagents, such as primers or antibodies, and precisely optimized experimental conditions for each target gene are necessary. To avoid such complicating steps, target genes can instead be tagged with various reporter genes for easier readout. When a target gene sequence is followed by the combined sequences of an internal ribosome entry site (IRES) and green fluorescence protein (GFP) in an expression vector, then the target gene and GFP are transcribed as a single mRNA and are translated independently in the cell [17,18]. Once an siRNA against the target gene is transduced together with the bicistronic expression vector, the siRNA will essentially destroy the entire mRNA, including the target gene and GFP. The GFP expression level is then expected to reflect the efficacy of the siRNA (Fig. 1).

Here, we utilized a GFP-expressing bicistronic vector to report the effect of an siRNA, and investigated whether the siRNA efficiency and specificity could be quantitatively monitored by flow cytometry.

Materials and methods

Cell culture. HEK293 cells were grown in Dulbecco's minimum essential medium supplemented with 10% fetal calf serum (FCS) at 37 °C in 100% humidified air.

siRNA design. siRNA sequences against the mouse cyclic AMP-responsive element modulator (CREM) gene were designed using the online siRNA design software programs siRNA Target Finder

* Corresponding author. Address: Department of Transfusion Medicine and Cell Therapy, Kyoto University Hospital, 54 Kawahara-cho, Shogoin, Sakyo-ku, Kyoto 606-8507, Japan. Fax: +81 75 751 4283.
E-mail address: hhirai@kuhp.kyoto-u.ac.jp (H. Hirai).
[1] These authors contributed equally to this work.

0006-291X/$ - see front matter © 2010 Elsevier Inc. All rights reserved.
doi:10.1016/j.bbrc.2010.02.033

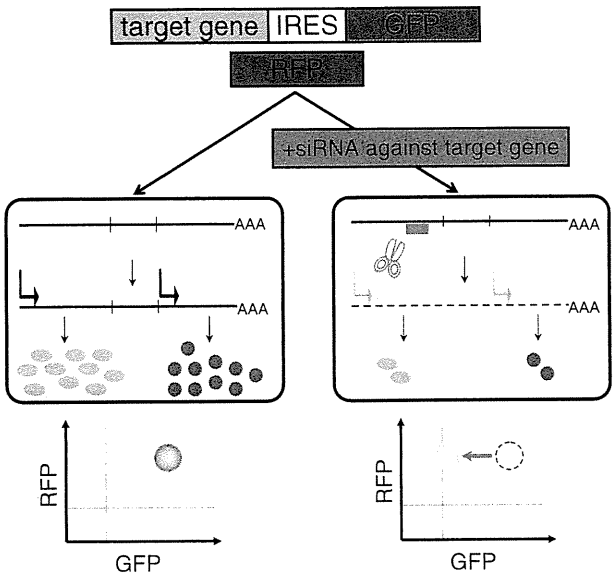

Fig. 1. Strategy and experimental design. The target gene and GFP are transcribed as a single mRNA from a bicistronic vector and translated independently (left panel). An siRNA against the target gene destroys the entire mRNA, including the target gene and GFP expressed from the bicistronic vector. The GFP expression level should reflect the effects of the siRNA (right panel). RFP is expressed from an independent vector.

(Ambion; http://www.ambion.com/jp/techlib/misc/siRNA_finder.html) and siDESIGN Center (Thermo Scientific; http://www.dharmacon.com/DesignCenter/DesignCenterPage.aspx). We chose three different 19-bp sequences that follow AA and contain GC sequences at less than a 50% frequency. The sequences were as follows: CREM#1, ggcaaatgaccatggaaa; CREM#2, gtaattgattcgcataaac; and CREM#3, gaagcaactcgcaagcggg. The siRNA sequences against firefly luciferase (GL3) and GFP were cttacgctgagtacttcga and caagctgaccctgaagttc, respectively.

Vector construction. Total RNA was extracted from a C57BL/6 mouse testis and reverse transcribed using the ReverTraAce kit (TOYOBO, Japan). The mouse CREM gene was amplified by PCR from the cDNA using the following primers: sense, gcgaattcatgagcaaatgtggcaggaaaaagtatatgagg; and anti-sense, ggctcggttactctgctttatggcaataa. The PCR product was digested with EcoRI and XhoI and cloned into the EcoRI–XhoI site of the retrovirus vector MSCV-IRES-GFP (pMIG). For red fluorescence protein (RFP) expression, pDsRed-Monomer-Hyg-N1 (pRFP, Clontech, CA) was used. The SiVM2 vector, in which a short hairpin RNA is driven by a human H1 promoter, was used for siRNA expression [19].

We used the following oligonucleotides encoding mouse CREM-specific siRNAs: (CREM#1), 5′-TCC CGG CAA ATG ACC ATG GAA ACT TCA AGA GAG TTT CCA TGG TCA TTT CCC T-3′ and 5′-GGC AAA TGA CTG GAA ACT CTC TTG AAG TTT CCA TGG TCA TTT GCC-3′; (CREM#2), 5′-TCC CGT AAT TGA TTC GCA TAA ACT TCA AGA GAG TTT ATG CGA ATC AAT TAC T-3′ and 5′-GTA ATT GAT TCG CAT AAA CTC TCT TGA AGT TTA TGC GAA TCA ATT AC-3′; and (CREM#3), 5′-TCC CGA AGC AAC TCG CAA GCG GGT TCA AGA GAC CCG CTT GCG AGT TGC TTC T-3′ and 5′-GAA GCA ACT CGC AAG CGG GTC TCT TGA ACC CGC TGC GAT TGC TTC-3′. These oligonucleotides were annealed and subcloned downstream of the H1 promoter using BbsI and XcmI in the SiVM2 vector [19].

Transfection. HEK293 cells were transduced with various combinations of plasmid vectors using the Lipofectamine LTX and Plus reagents (Invitrogen, CA) according to the manufacturer's protocol. Briefly, cells were seeded 24-h prior to transfection into a 6-well plate at a density of 1×10^5/well. One microgram of DNA was mixed with 2.5 μl of Lipofectamine LTX and 1 μl of Plus reagent in 200 μl of OPTI-MEM medium, incubated at room temperature for 30 min, and then added to each well of the 6-well plate. The fluorescence of GFP and RFP were monitored using an Olympus IX71 microscope, and data were captured with DP controller/Manager software (Olympus, Japan).

Flow cytometry. Twenty-four hours after transfection, the cells were washed with phosphate buffered saline (PBS), treated with 0.05% trypsin/EDTA, and resuspended in PBS supplemented with 2% FCS. Flow cytometric analysis was carried out using FACSCalibur (BD). To calibrate our flow cytometry results, mock-transfected cells and cells transduced with either pMIG or pRFP alone were included with every experiment. Data were analyzed using FlowJo software (Tree Star, Inc.).

Real-time PCR. RNA was extracted from cells using the RNeasy Micro kit (Qiagen) according to the manufacturer's protocol, and was reverse transcribed using a random hexamer primer. Quantitative PCR was performed using the Light Cycler Taqman Master kit (Roche). The CREM expression was normalized to GAPDH expression. The primers and probes used were as follows: (mouse CREM) left, gctgaggctgatgaaaaaca, right, gccacacgattttcaagaca, universal probe library (UPL) #4; (GAPDH) left, tgtccgtcgtggatctac, right, cctgcttcaccaccttcttg, UPL #80.

Western blotting. We used anti-CREM (sc-440 X, Santa Cruz), anti-actin (sc7210, Santa Cruz), and HRP-conjugated anti-rabbit (sc-2317, Santa Cruz) antibodies for Western blotting. Band intensities were quantified using Image J software (http://rsb.info.nih.gov/ij/).

Results

To verify that the GFP expression level could be evaluated by flow cytometry, we first examined siRNA directly targeted to GFP. An MSCV-based vector (MSCV-IRES-GFP: pMIG) was utilized as our GFP expression vector. An siRNA sequence against GFP was cloned into the siVM2 expression vector, in which siRNA was driven by a human H1 promoter (siVM2GFP) [19]. A red RFP monomer expression vector (pDsRed-Momoner-Hyg-N1: pRFP) was used to normalize the transduction efficiency.

HEK293 cells were transduced with pRFP and pMIG with or without siVM2GFP, and the GFP and RFP expression levels were evaluated by fluorescent microscopy and flow cytometry 24 h after transfection (Fig. 2A and B, respectively). When the RFP expression vector was co-transduced with GFP, most RFP-positive cells expressed GFP, as expected (middle panels in Fig. 2A and B). The GFP expression was highly suppressed when siVM2GFP was co-transduced (bottom panels in Fig. 2A and B). In contrast, the RFP expression level was not affected by addition of the GFP-targeted siRNA expression vector, suggesting that the use of RFP is appropriate for correcting the transduction efficiency.

Fig. 2C displays the mean fluorescent intensities (MFIs) for GFP within RFP-positive cells. The solid and dotted lines represent GFP expression with or without the GFP expression vector, respectively, while the shaded line represents GFP expression in RFP-positive cells transduced with the siRNA expression vector. The MFIs for each condition were: 5.06 for pRFP only, 226 for pMIG + pRFP, and 37.5 for siVM2GFP + pMIG + pRFP. The siRNA efficiency was calculated as 85.3%, according to the following equation: siRNA efficiency = (MFIpMIG + pRFP − MFIpMIG + pRFP + siVM2)/(MFIpMIG + pRFP − MFIpRFPonly). These results suggest that the GFP expression level within RFP-positive cells could be examined at the single cell level by flow cytometry.

Using this system, we assessed three different siRNA sequences targeting the mouse CREM protein. CREM is a member of the cyclic

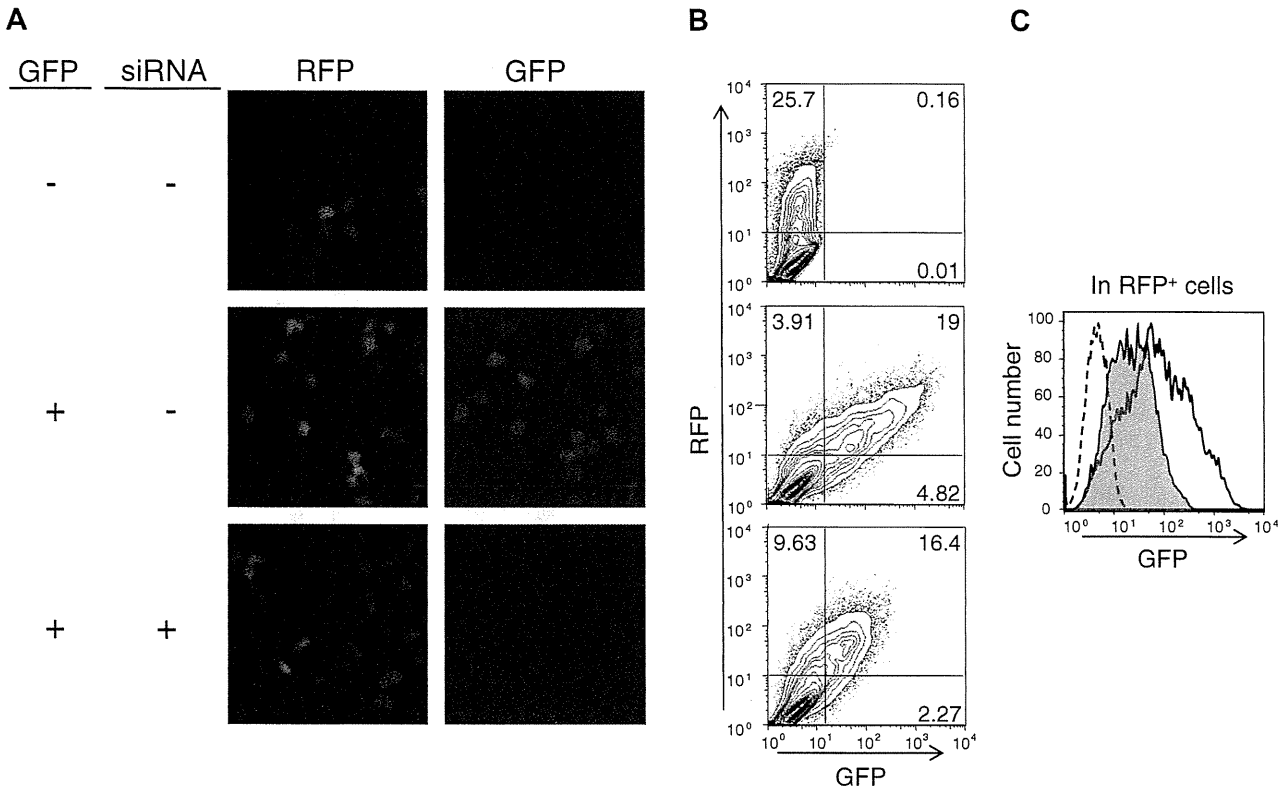

Fig. 2. Flow cytometry-based quantification of GFP expression using GFP-targeted siRNA. HEK293 cells were transduced with an RFP expression vector, co-transduced with or without a GFP and/or an siRNA expression vector, as indicated. Fluorescence was monitored 24 h after transduction by fluorescent microscopy (A) or flow cytometry (B and C). The mean fluorescent intensities (MFI) of GFP in the RFP-positive cells were plotted in (C). The solid and dotted lines represent GFP expression within RFP-positive cells with or without the GFP expression vector, respectively. The GFP expression levels with the siRNA expression vectors are represented by the shaded lines. Results are representative of three independent experiments.

AMP responsive element binding (CREB) protein family of transcription factors. The siRNAs were designed to target the mouse CREM (NM_013498) coding sequence at 308-, 469-, and 817-bp. As a non-specific siRNA control, we used siRNA targeted to firefly luciferase (GL3, Promega). Fig. 3A shows the GFP and RFP expression levels in cells transduced with a GFP expression vector without mouse CREM sequences (pMIG). None of the siRNAs affected the GFP or RFP expression levels (Fig. 3A, left panel). The solid and dotted lines in Fig. 3A (right panels) represent the GFP expression in RFP-positive cells with or without pMIG, respectively. The shaded lines represent the GFP expression levels with transduction of the siRNA expression vectors. The GFP expression within RFP-positive cells was not repressed by any siRNA vector.

Next, HEK293 cells were transduced with pRFP and a bicistronic CREM expression vector (pMIG-mCREM), with or without an siRNA expression vector. CREM-targeted, but not luciferase-targeted, siRNAs specifically repressed GFP expression (Fig. 3B, left panels). The GFP expression levels of RFP-positive cells are plotted in the right panels of Fig. 3B. The solid and dotted lines represent GFP expression within RFP-positive cells transduced with or without pMIG-mCREM, respectively. The shaded lines represent GFP expression with transduction of the siRNA expression vectors. The MFIs for each condition were as follows: 6.19 for pRFP only, 59 for pMIG-mCREM + pRFP, 46.4 for pMIG-mCREM + pRFP + siVM2GL3, 9.59 for pMIG-mCREM + pRFP + siVM2CREM#1, 8.88 for pMIG-mCREM + pRFP + siVM2CREM#2, and 14.8 for pMIG-mCREM + pRFP + siVM2CREM#3 (Fig. 3B, right panels). All three siRNA sequences targeting mouse CREM (CREM#1, #2, and #3) effectively suppressed GFP expression in RFP-positive cells compared to the control (no siRNA expression vector), with efficiencies of 93.5%, 94.9%, and 83.6%, respectively. The siRNA for firefly luciferase did not affect GFP expression. These results suggest that the effects of the siRNA vectors on the GFP expression level were specific to the CREM sequence located in front of the IRES sequence, and not to the GFP sequence.

To verify our screening method, we measured the mRNA and protein expression levels using real-time PCR and Western blotting, respectively (Fig. 4B–D). The total RNAs and proteins for the measurement were extracted from the same samples as used in the flow cytometric analysis. Both the mRNA and protein expression levels of CREM correlated very well with the relative MFI for GFP in RFP-positive cells (Fig. 4E and F, $R^2 = 0.9537$ and 0.9171, respectively). We also verified the feasibility of the system by applying it to four other genes (data not shown).

Discussion

In this study, we successfully evaluated the efficacy and specificity of siRNAs by monitoring the fluorescent proteins expressed from bicistronic vectors by flow cytometry.

Various reporter genes have been utilized for siRNA screening [20–24]. The advantages of using targeted reporter genes over direct measurements are many. For instance, the siRNA efficiency can be evaluated even when target gene-specific reagents such as antibodies are not available. Furthermore, when a target gene is expressed at very low levels by the cells, the effect of an siRNA can be difficult to evaluate by direct measurement of the RNA or proteins. Enhancement of target gene expression by vectors en-

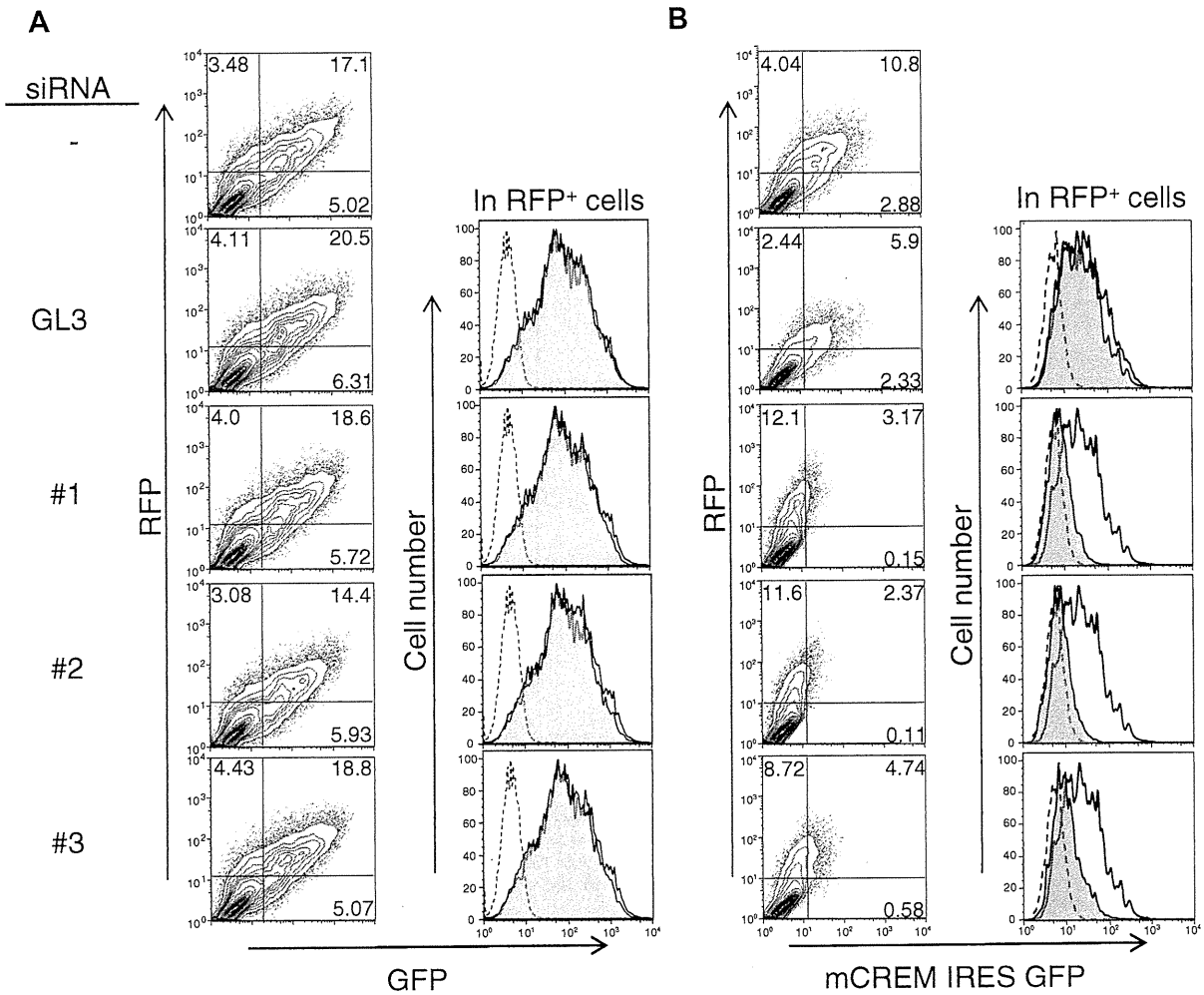

Fig. 3. Flow cytometry-based method for screening for an effective siRNA against the mouse CREM gene. (A) HEK293 cells were transduced with an RFP vector and a GFP expression vector with or without one of the siRNA expression vectors (firefly luciferase [GL3], CREM#1, CREM#2, or CREM#3). Flow cytometry data analyzed 24 h after transduction are shown in the left panels. The RFP-positive cells (left panels) were analyzed for GFP expression (right panels). The solid and dotted lines represent GFP expression within RFP-positive cells with or without pMIG, respectively. (B) HEK293 cells were transduced with the pRFP vector and a bicistronic CREM expression vector (CREM + GFP) with or without one of the siRNA expression vectors (firefly luciferase [GL3], CREM#1, CREM#2, or CREM#3). Results are representative of three independent experiments.

ables us to avoid such problems. Low transduction efficiencies also complicate the evaluation of the effects of an siRNA. Direct measurements typically assess the gene expression level in a cell mass, and not on an individual cell basis. By using flow cytometry, fluorescent proteins of multiple wavelengths can be monitored simultaneously after the simple manipulation of cells [24]. The intensities of the multiple fluorescences from a single cell can be quantitatively monitored and recorded. In this study, fluorescence intensities representing the efficacy of siRNAs (GFP) and the transduction (RFP) were monitored simultaneously from a single cell by flow cytometry, resulting in single cell-based quantification. By monitoring the GFP level of RFP-positive cells, problems arising from low transduction efficiencies could be avoided. Flow cytometric analyses were performed 24 h after transfection, and did not require RNA or protein extractions, which are time- and labor-consuming processes. Cells were simply treated with trypsin and EDTA and then directly analyzed. Each process step was very simple and was performed within a fairly short time. These features of the experimental process are suitable for high-throughput assay.

We utilized bicistronic expression vectors to indicate target gene expression rather than target-fused fluorescent reporter genes. Bicistronic vectors are already widely used in many fields, and cloning is easier to perform than the fusion process. The stability of GFP expressed from a bicistronic vector is theoretically constant irrespective of the target genes. Optimization of the time course of the experiment is unnecessary because of the consistency of protein stability. In addition, GFP repression by an siRNA against a target gene is mediated at the mRNA level and not after translation, since the target gene and GFP are transcribed as a single mRNA and are translated in different ways (cap-dependent and -independent translation, respectively) [25,26]. Therefore, RNA interference-dependent gene silencing can be more precisely monitored than is possible using the fusion system.

In summary, we have devised a novel flow cytometry-based method to evaluate the effects of siRNAs. Cell samples for flow cytometry are prepared by transducing siRNA and a bicistronic vector, which expresses GFP and the target gene, together with an RFP expression vector. The simplicity of this flow cytometry-

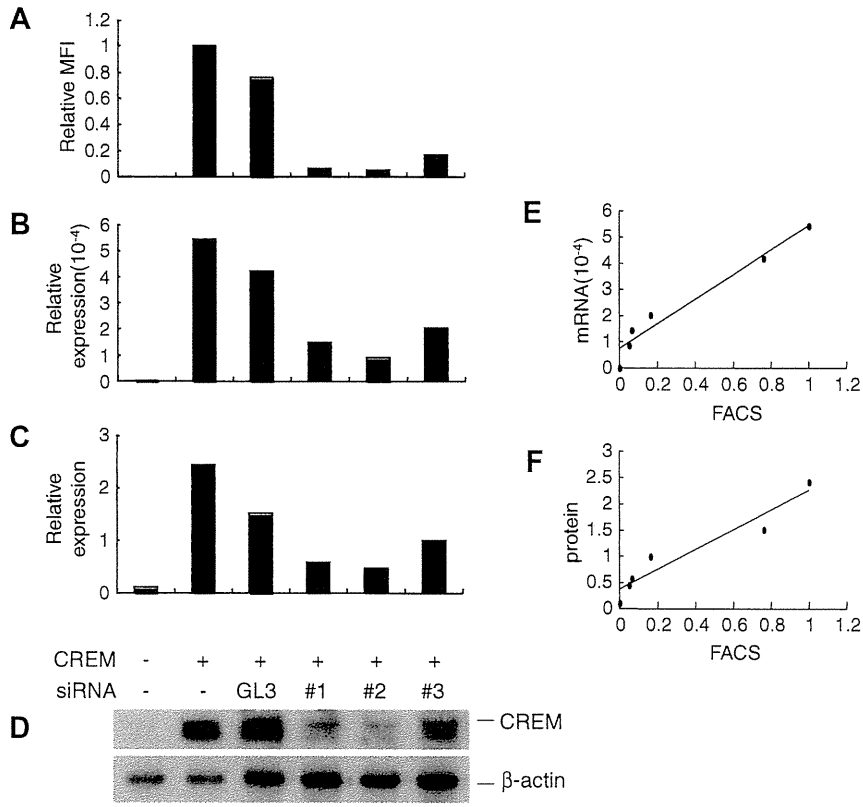

Fig. 4. Verification of the flow cytometry-based method by conventional methods. HEK293 cells were transduced with an RFP vector and a bicistronic CREM expression vector (CREM + GFP), with or without one of the siRNA expression vectors (firefly luciferase [GL3], CREM#1, CREM#2, or CREM#3). (A) Flow cytometric analysis 24 h after transduction. Mean fluorescent intensities of GFP in RFP-positive cells. (B) Relative expression level of mRNA for the mouse CREM gene, normalized to GAPDH. (C and D) Western blotting results. The band densities in (D) were quantified using Image J software (C). (E and F) The MFI was correlated with the mRNA (R^2 = 0.9537) (E) or protein expression (R^2 = 0.9171) (F). Results are representative of three independent experiments.

based method will facilitate the screening of effective siRNA sequences.

Acknowledgments

We thank Drs. S. Mizuno and K. Akashi for generously providing us with siVM2 vector. This work was supported by the Mitsubishi Foundation to H.H.; and Kakenhi [Grant Nos. 21591246 to H.H. and 21590443 to J.I.].

References

[1] A. Fire, S. Xu, M.K. Montgomery, S.A. Kostas, S.E. Driver, C.C. Mello, Potent and specific genetic interference by double-stranded RNA in *Caenorhabditis elegans*, Nature 391 (1998) 806–811.
[2] D.M. Dykxhoorn, C.D. Novina, P.A. Sharp, Killing the messenger: short RNAs that silence gene expression, Nat. Rev. Mol. Cell Biol. 4 (2003) 457–467.
[3] T. Tuschl, A. Borkhardt, Small interfering RNAs: a revolutionary tool for the analysis of gene function and gene therapy, Mol. Interv. 2 (2002) 158–167.
[4] P.J. Paddison, J.M. Silva, D.S. Conklin, M. Schlabach, M. Li, S. Aruleba, V. Balija, A. O'Shaughnessy, L. Gnoj, K. Scobie, K. Chang, T. Westbrook, M. Cleary, R. Sachidanandam, W.R. McCombie, S.J. Elledge, G.J. Hannon, A resource for large-scale RNA-interference-based screens in mammals, Nature 428 (2004) 427–431.
[5] Y. Dorsett, T. Tuschl, SiRNAs: applications in functional genomics and potential as therapeutics, Nat. Rev. Drug Discov. 3 (2004) 318–329.
[6] G.J. Hannon, J.J. Rossi, Unlocking the potential of the human genome with RNA interference, Nature 431 (2004) 371–378.
[7] E. Ashihara, E. Kawata, T. Maekawa, Future prospects of RNA interference for cancer therapies, Curr. Drug Targets, in press..
[8] L.J. Scherer, J.J. Rossi, Approaches for the sequence-specific knockdown of mRNA, Nat. Biotechnol. 21 (2003) 1457–1465.
[9] T. Holen, M. Amarzguioui, M.T. Wiiger, E. Babaie, H. Prydz, Positional effects of short interfering RNAs targeting the human coagulation trigger tissue factor, Nucleic Acids Res. 30 (2002) 1757–1766.
[10] Q. Du, H. Thonberg, J. Wang, C. Wahlestedt, Z. Liang, A systematic analysis of the silencing effects of an active siRNA at all single-nucleotide mismatched target sites, Nucleic Acids Res. 33 (2005) 1671–1677.
[11] D.S. Schwarz, H. Ding, L. Kennington, J.T. Moore, J. Schelter, J. Burchard, P.S. Linsley, N. Aronin, Z. Xu, P.D. Zamore, Designing siRNA that distinguish between genes that differ by a single nucleotide, PLoS Genet. 2 (2006) e140.
[12] A. Reynolds, D. Leake, Q. Boese, S. Scaringe, W.S. Marshall, A. Khvorova, Rational siRNA design for RNA interference, Nat. Biotechnol. 22 (2004) 326–330.
[13] M. Amarzguioui, H. Prydz, An algorithm for selection of functional siRNA sequences, Biochem. Biophys. Res. Commun. 316 (2004) 1050–1058.
[14] Y. Naito, T. Yamada, K. Ui-Tei, S. Morishita, K. Saigo, siDirect: highly effective, target-specific siRNA design software for mammalian RNA interference, Nucleic Acids Res. 32 (2004) W124–W129.
[15] K. Ui-Tei, Y. Naito, F. Takahashi, T. Haraguchi, H. Ohki-Hamazaki, A. Juni, R. Ueda, K. Saigo, Guidelines for the selection of highly effective siRNA sequences for mammalian and chick RNA interference, Nucleic Acids Res. 32 (2004) 936–948.
[16] W. Li, L. Cha, Predicting siRNA efficiency, Cell. Mol. Life Sci. 64 (2007) 1785–1792.
[17] P. de Felipe, Polycistronic viral vectors, Curr. Gene Ther. 2 (2002) 355–378.
[18] S.M. Ngoi, A.C. Chien, C.G. Lee, Exploiting internal ribosome entry sites in gene therapy vector design, Curr. Gene Ther. 4 (2004) 15–31.
[19] H. Hirai, P. Zhang, T. Dayaram, C.J. Hetherington, S. Mizuno, J. Imanishi, K. Akashi, D.G. Tenen, C/EBPbeta is required for 'emergency' granulopoiesis, Nat. Immunol. 7 (2006) 732–739.
[20] R. Kumar, D.S. Conklin, V. Mittal, High-throughput selection of effective RNAi probes for gene silencing, Genome Res. 13 (2003) 2333–2340.
[21] Q. Du, H. Thonberg, H.Y. Zhang, C. Wahlestedt, Z. Liang, Validating siRNA using a reporter made from synthetic DNA oligonucleotides, Biochem. Biophys. Res. Commun. 325 (2004) 243–249.
[22] N. Smart, P.J. Scambler, P.R. Riley, A rapid and sensitive assay for quantification of siRNA efficiency and specificity, Biol. Proced. Online 7 (2005) 1–7.

[23] C.F. Hung, K.C. Lu, T.L. Cheng, R.H. Wu, L.Y. Huang, C.F. Teng, W.T. Chang, A novel siRNA validation system for functional screening and identification of effective RNAi probes in mammalian cells, Biochem. Biophys. Res. Commun. 346 (2006) 707–720.
[24] H.Y. Ho, M.L. Cheng, Y.H. Wang, D.T. Chiu, Flow cytometry for assessment of the efficacy of siRNA, Cytometry A 69 (2006) 1054–1061.
[25] E. Martinez-Salas, Internal ribosome entry site biology and its use in expression vectors, Curr. Opin. Biotechnol. 10 (1999) 458–464.
[26] M. Stoneley, A.E. Willis, Cellular internal ribosome entry segments: structures, trans-acting factors and regulation of gene expression, Oncogene 23 (2004) 3200–3207.

Activity of the multitargeted kinase inhibitor, AT9283, in imatinib-resistant BCR-ABL–positive leukemic cells

*Ruriko Tanaka,[1] *Matthew S. Squires,[2] Shinya Kimura,[1,3] Asumi Yokota,[1] Rina Nagao,[1] Takahiro Yamauchi,[4] Miki Takeuchi,[1] Hisayuki Yao,[1] Matthias Reule,[2] Tomoko Smyth,[2] John F. Lyons,[2] Neil T. Thompson,[2] Eishi Ashihara,[1] Oliver G. Ottmann,[5] and Taira Maekawa[1]

[1]Department of Transfusion Medicine and Cell Therapy, Kyoto University Hospital, Kyoto, Japan; [2]Astex Therapeutics Ltd, Cambridge, United Kingdom; [3]Division of Hematology, Respiratory Medicine, and Oncology, Saga University, Saga, Japan; [4]Department of Hematology and Oncology, Faculty of Medical Sciences, University of Fukui, Fukui, Japan; and [5]Department of Hematology, Johann Wolfgang Goethe University, Frankfurt, Germany

Despite promising clinical results from imatinib mesylate and second-generation ABL tyrosine kinase inhibitors (TKIs) for most BCR-ABL$^+$ leukemia, BCR-ABL harboring the mutation of threonine 315 to isoleucine (BCR-ABL/T315I) is not targeted by any of these agents. We describe the in vitro and in vivo effects of AT9283 (1-cyclopropyl-3[5-morpholin-4yl methyl-1H-benzomidazol-2-yl]-urea), a potent inhibitor of several protein kinases, including Aurora A, Aurora B, Janus kinase 2 (JAK2), JAK3, and ABL on diverse imatinib-resistant BCR-ABL$^+$ cells. AT9283 showed potent antiproliferative activity on cells transformed by wild-type BCR-ABL and BCR-ABL/T315I. AT9283 inhibited proliferation in a panel of BaF3 and human BCR-ABL$^+$ cell lines both sensitive and resistant to imatinib because of a variety of mechanisms. In BCR-ABL$^+$ cells, we confirmed inhibition of substrates of both BCR-ABL (signal transducer and activator of transcription-5) and Aurora B (histone H3) at physiologically achievable concentrations. The in vivo effects of AT9283 were examined in several mouse models engrafted either subcutaneously or intravenously with BaF3/BCR-ABL, human BCR-ABL$^+$ cell lines, or primary patient samples expressing BCR-ABL/T315I or glutamic acid 255 to lysine, another imatinib-resistant mutation. These data together support further clinical investigation of AT9283 in patients with imatinib- and second-generation ABL TKI-resistant BCR-ABL$^+$ cells, including T315I. (*Blood*. 2010;116(12): 2089-2095)

Introduction

Philadelphia (Ph) chromosome results from a reciprocal translocation between chromosomes 9 and 22 and generates the BCR-ABL chimera protein, the cause of chronic myeloid leukemia (CML) and Ph$^+$ acute lymphoid leukemia (ALL). The ABL tyrosine kinase inhibitor (TKI), imatinib mesylate, has dramatically changed the first-line therapy of CML.[1] Most patients with newly diagnosed CML with chronic phase, when treated with imatinib, achieve durable responses. However, emergence of refractory disease and relapse have frequently been reported, particularly in patients with CML with advanced-stage disease and patients with Ph$^+$ ALL.[2,3] Among several mechanisms of resistance, point mutations within the ABL kinase domain that interfere with imatinib binding are the most critical cause of imatinib resistance.[4,5]

To overcome these imatinib resistance mechanisms, 4 second-generation ABL TKIs have been developed: dasatinib,[6] nilotinib,[7] bosutinib[8] and bafetinib (formerly INNO-406).[9,10] Despite promising clinical results from these second-generation ABL TKIs for most patients with imatinib-resistant BCR-ABL$^+$ leukemia, the mutation of threonine 315 to isoleucine (T315I) confers resistance to all these TKIs.[11,12] Thus, identification of novel agents for the effective treatment of patients with CML with T315I is an important and challenging task.[13] Aurora kinases A and B are a family of serine/threonine kinases involved in many cellular functions.[14-16] Inappropriate expression of these enzymes in certain cancers may result in aneuploidy and carcinogenesis.[17] Consequently, the potential therapeutic value of targeting Aurora kinases has become a focus of anticancer therapy.[14]

Recently, we identified an Aurora kinase inhibitor, AT9283 (1-cyclopropyl-3[5-morpholin-4yl methyl-1H-benzomidazol-2-yl]-urea) by way of structure-based optimization of a ligand-efficient pyrazole-benzimidazole fragment. X-ray crystallographic structures were generated with the use of a novel soakable form of Aurora A and were used to drive the optimization toward potent (half-maximal inhibition constant [IC_{50}] < 3nM) dual Aurora A/B inhibitor. AT9283 that also potently inhibits several kinases, including Janus kinase-2 (JAK2) and JAK3 (1.2 and 1.1nM, respectively), c-ABL (110nM), and ABL/T315I (4nM), is currently under evaluation in phase 1 clinical trials for metastatic solid tumors and hematologic malignancies.[18,19]

Here, we report the putative mechanism by which AT9283 binds to BCR-ABL/T315I and its activity against imatinib-resistant BCR-ABL$^+$ leukemic cells, including those with the T315I mutation.

Methods

Reagent and cell lines

AT9283 was synthesized by Astex Therapeutics Ltd (Figure 1A).[18] Human CML cell lines (K562, MEG-01, BV173, KU812, MYL, KT-1, and

Submitted March 17, 2009; accepted May 10, 2010. Prepublished online as *Blood* First Edition paper, June 14, 2010; DOI 10.1182/blood-2009-03-211466.

*R.T. and M.S.S. contributed equally to this study.

The online version of this article contains a data supplement.

The publication costs of this article were defrayed in part by page charge payment. Therefore, and solely to indicate this fact, this article is hereby marked "advertisement" in accordance with 18 USC section 1734.

KBM-5), human acute myeloid leukemia cell lines (HL60, KG1a), human ALL (Jurkat, Nalm6), and mouse pro-B cell line (BaF3) were used. KBM-5/STIR, which was the subclone of KBM-5 with T315I, and BaF3/wild type (wt) BCR-ABL^{p190} were also used. Source of all cell lines used are outlined in supplemental Table 1 (available on the *Blood* Web site; see the Supplemental Materials link at the top of the online article). BaF3/wt-BCR-ABL^{p210} and BaF3 cells harboring imatinib-resistant mutations (glycine 250 to glutamic acid, glutamine 252 to histidine, tyrosine 253 to phenylalanine, glutamic acid 255 to lysine [E255K]), methionine 294 to valine, T315I, threonine 315 to alanine, phenylalanine 317 to leucine, phenylalanine 317 to valine, methionine 351 to threonine, and histidine 396 to proline) in the BCR-ABL^{p210} kinase domain were established as previously described.[9] All cell lines were cultured in RPMI 1640 (Nissui) with 2mM L-glutamine (Nacalai Tesque) and 10% fetal bovine serum (Vitromex) and were maintained at 37°C in a fully humidified atmosphere of 5% CO_2. For the culture of parental BaF3 cells, 1 ng/mL murine interleukin-3 (Sigma-Aldrich) was added to the medium. Cells undergoing exponential growth were used in the experiments.

Bone marrow cells from healthy donors and patients with CML in chronic phase were collected with written informed consents according to the Declaration of Helsinki. Primary leukemic cells were obtained from 2 patients with Ph$^+$ ALL who relapsed after imatinib mesylate treatment because of E255K or T315I.[20] These patients' peripheral blood contained more than 90% leukemic cells. Approval for primary leukemic cells was obtained from the institutional review board at Frankfurt University Hospital.

Docking model of AT9283 bound within the active site of c-ABL/T315I

A model of c-ABL/T315I was prepared in QUANTA (Accelrys Inc) by simple Thr>Ile mutation of residue 315 in an inhouse DFG-in, wt c-ABL structure. Docking of AT9283 into the active site of the c-ABL/T315I model was carried out with the use of a proprietary version of GOLD,[21] using the Chemscore scoring function.[22]

Proliferation assays

Proliferation of the cell lines was determined with a modified 3-(4,5-dimethylthiazol -2-yl)-2,5-diphenyl-2H tetrazolium bromide assay with the SF reagent (Nacalai Tesque) as previously described.[23] Leukemic cell lines were cultivated in a flat-bottomed 96-well plate (Greiner Labortechnik) at 1×10^4 (BaF3 series), 5×10^4 (BV173, KBM-5, KBM-5/STIR), or 1×10^5 (MEG01, KU812, HL60) cells per well in 100 μL of medium and incubated with various concentrations of AT9283 for 72 hours. The means of 5 data values for each treatment were calculated. IC_{50}s were determined with the use of the nonlinear regression program CalcuSyn (Biosoft).[24]

Western blotting

BCR-ABL$^+$ or BCR-ABL$^-$ cell lines were seeded at a concentration of 1×10^6/mL media onto 6-well tissue culture plates and allowed to recover for 16 hours. AT9283, at the indicated concentration, or vehicle control (0.1% dimethyl sulfoxide) were added for 24 hours. Cells were harvested and lysed in 100 μL of ice-cold Triton lysis buffer (0.1% vol/vol Tx-100). Lysates were cleared by centrifugation, and a sample of the supernatant was removed for protein determination. Equivalent amounts of protein lysate had sodium dodecylsulfate sample buffer added and were boiled for 5 minutes. Samples were resolved by sodium dodecylsulfate–polyacrylamide gel electrophoresis (NuPage system; Invitrogen) and blotted onto polyvinylidene difluoride filters. Immunoblotting was performed with specific antibodies for phospho (p) histone H3 (HH3)$^{(Ser10)}$ and total (t)HH3, p signal transducer and activator of transcription-5 (STAT5)$^{(Tyr694)}$, tSTAT5, pCrkL$^{(Tyr207)}$, tCrkL, p extracellular signal-regulated kinase (ERK)$^{(Thr202/Tyr204)}$, tERK, pAKT$^{(Thr308)}$, tAKT, pBCR-ABL$^{(Tyr177)}$, tBCR-ABL, pAurora A$^{(Thr288)}$, tAurora A, pAuroa B$^{(Thr232)}$, and tAurora B. All antibodies were obtained from Cell Signaling Technology. Detection was achieved with the use of Odyssey Infra Red Imaging, IR Dye secondary antibodies, and a Licor Odyssey Imager (Li-Cor Bioscience Ltd).

In vivo activity of AT9283 in mice bearing BCR-ABL$^+$ leukemic cells

BaF3/wt-BCR-ABL^{p210}, BaF3/T315I, or human CML K562 xenografts used male BALB/c nu/nu mice and were performed according to the United Kingdom Animals (Scientific Procedures) Act 1986. Animals were purchased from Harlan UK Ltd and housed in pathogen-free conditions. Six- to 8-week-old male BALB/c Hsd:athymic nude-*Foxn1*^{nu} mice were implanted subcutaneously with 1×10^7 BaF3/wt-BCR-ABL, 1×10^7 BaF3/T315I, or 1×10^7 K562 cells per mouse into the right flank. Five days after implantation mice were arranged into groups of 8 according to tumor volume with a mean volume of 100 mm^3. AT9283 was prepared in a vehicle of 10% dimethyl sulfoxide, 20% water, and 70% 2-(hydroxypropyl)-beta-cyclodextrin (25% wt/vol). Mice were then dosed according to schedule. Tumor volume was measured every 2 to 3 days. In each case a statistically significant slowing of increase in xenograft volume or regression of tumor volume over time compared with a matched control group was used to characterize efficacy. A complete regression was defined as a decrease in tumor volume to an undetectable size, taken as measurements of less than 3 mm in any dimension. Tolerability was estimated by standard criteria of behavioral observations, body weight loss less than 5%, and survival over the course of the study.

For the experiments to investigate the effects of AT9283 on the primary patient samples with BCR-ABL harboring E255K or T315I, nonobese diabetic/severe combined immunodeficient (NOD/SCID) mice were used with the approval from the institutional review board at Kyoto University Hospital. Male NOD/SCID mice 4 to 6 weeks of age (Japan Clea) were individually sublethally irradiated (2 Gy) and inoculated intravenously with 5.0×10^5 primary leukemic cells harboring either BCR-ABL/E255K or T315I as previously described.[20] Briefly, engraftments of inoculated primary human BCR-ABL$^+$ cells at day 7 after transplantation were confirmed by polymerase chain reaction analysis, and treatments with AT9283 were initiated on day 7. Furthermore, the numbers of engrafted BCR-ABL$^+$ cells were monitored by analysis of the percentage of human leukemic cells in mouse peripheral blood by flow cytometry as previously described.[20,23] The mice were randomized into the following groups: E255K [each group, n = 7, as follows: (1) untreated mice, (2) mice treated with 6.25 mg/kg AT9283 twice daily] and T315I [each group, n = 5, as follows: (1) untreated mice, (2) mice treated with 10 mg/kg AT9283 daily, and (3) mice treated with 15 mg/kg AT9283 daily]. At day 7, treatment was administered intraperitoneally either twice daily 5 days on and 2 days off for 4 weeks at the doses of 6.25 mg/kg (E255K) or daily 4 days on and 3 days off continuously at the doses of 10 mg/kg and 15 mg/kg (T315I). For survival analysis, death was determined either by spontaneous death or elective killing because of pain or suffering according to established criteria.

Results

Identification and in vitro activity of AT9283

By analogy with the binding mode of AT9283 with Aurora A,[18] it is predicted that AT9283 does not form a hydrogen bond with T315 in BCR-ABL in the way that inhibitors, including imatinib, do. Binding of AT9283 is therefore less likely to be affected by the T315I mutation (supplemental Figure 1A). Furthermore, AT9283 does not bind within the selectivity pocket behind the gatekeeper residue, meaning that its potency for ABL kinase is not abrogated by mutation of this residue to the bulkier isoleucine. Imatinib binding is sterically hindered by the presence of isoleucine at amino acid 315, whereas AT9283 is not (Figure 1B).

Cell-based activity of AT9283 in BCR-ABL–dependent cell lines

AT9283 inhibited proliferation of a panel of BaF3 cell lines transformed with either wt-BCR-ABL fusions or a variety of mutant forms, including T315I (Table 1). AT9283 inhibited all lines